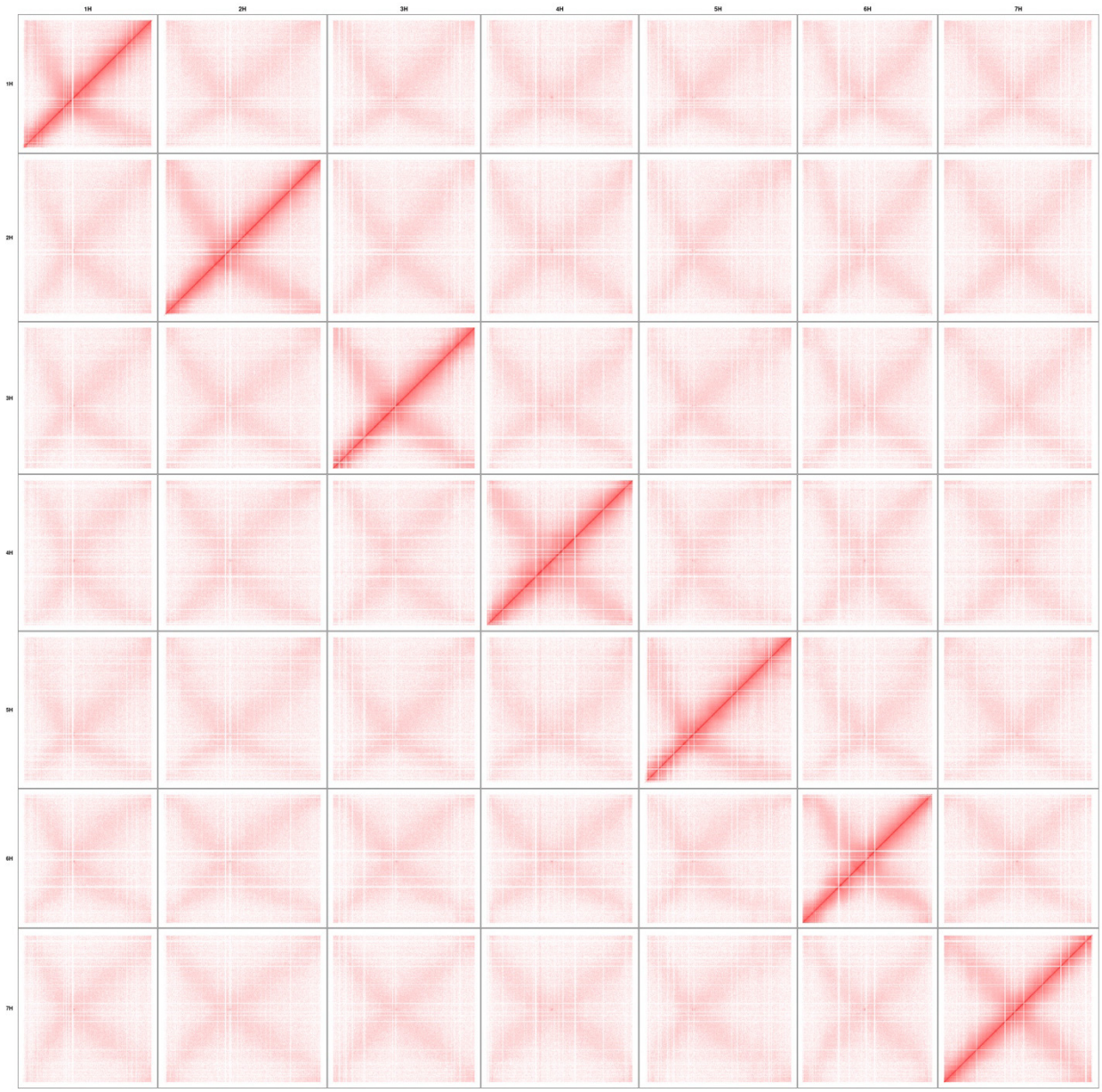

Supplementary Figure 1: *H. bogdanii* H240 Hi-C contact matrix. The intensity of pixels represents the normalized count of Hi-C links between 1 Mb windows on all chromosomes and haplotypes.

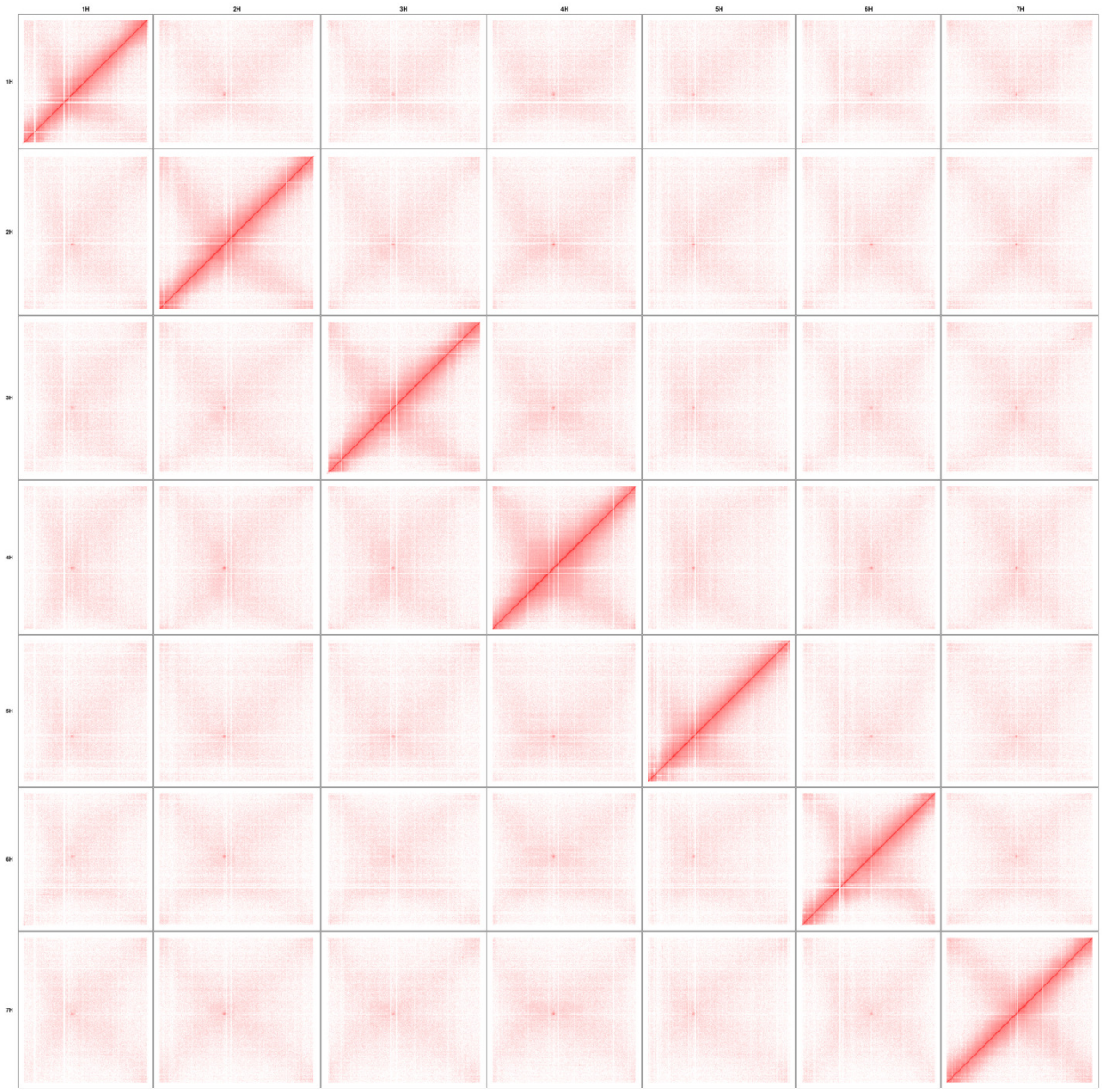

Supplementary Figure 2: *H. brevisubulatum* PI401390 Hi-C contact matrix. The intensity of pixels represents the normalized count of Hi-C links between 1 Mb windows on all chromosomes and haplotypes.

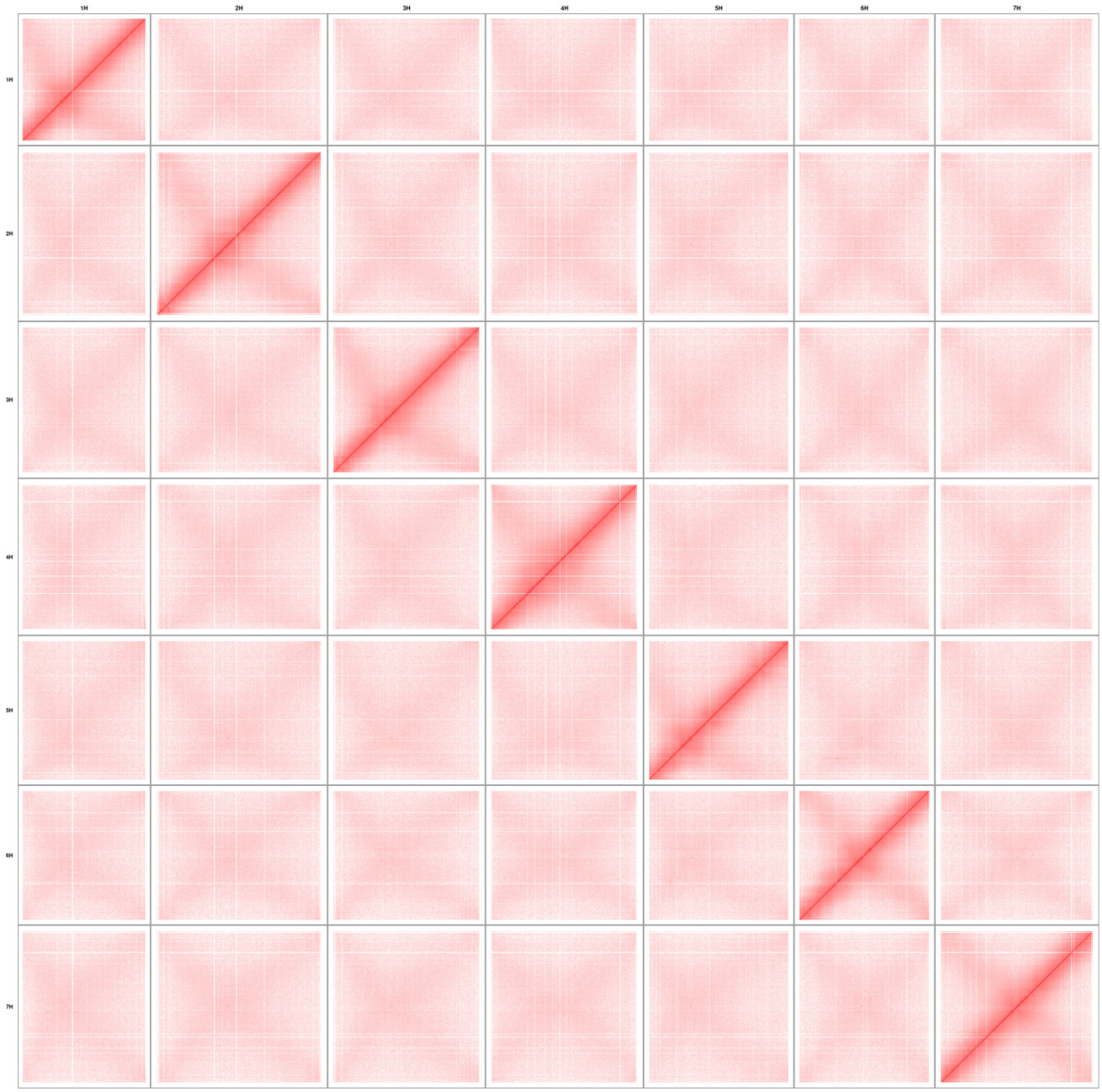

Supplementary Figure 3: *H. californicum* BCC2058 Hi-C contact matrix. The intensity of pixels represents the normalized count of Hi-C links between 1 Mb windows on all chromosomes and haplotypes.

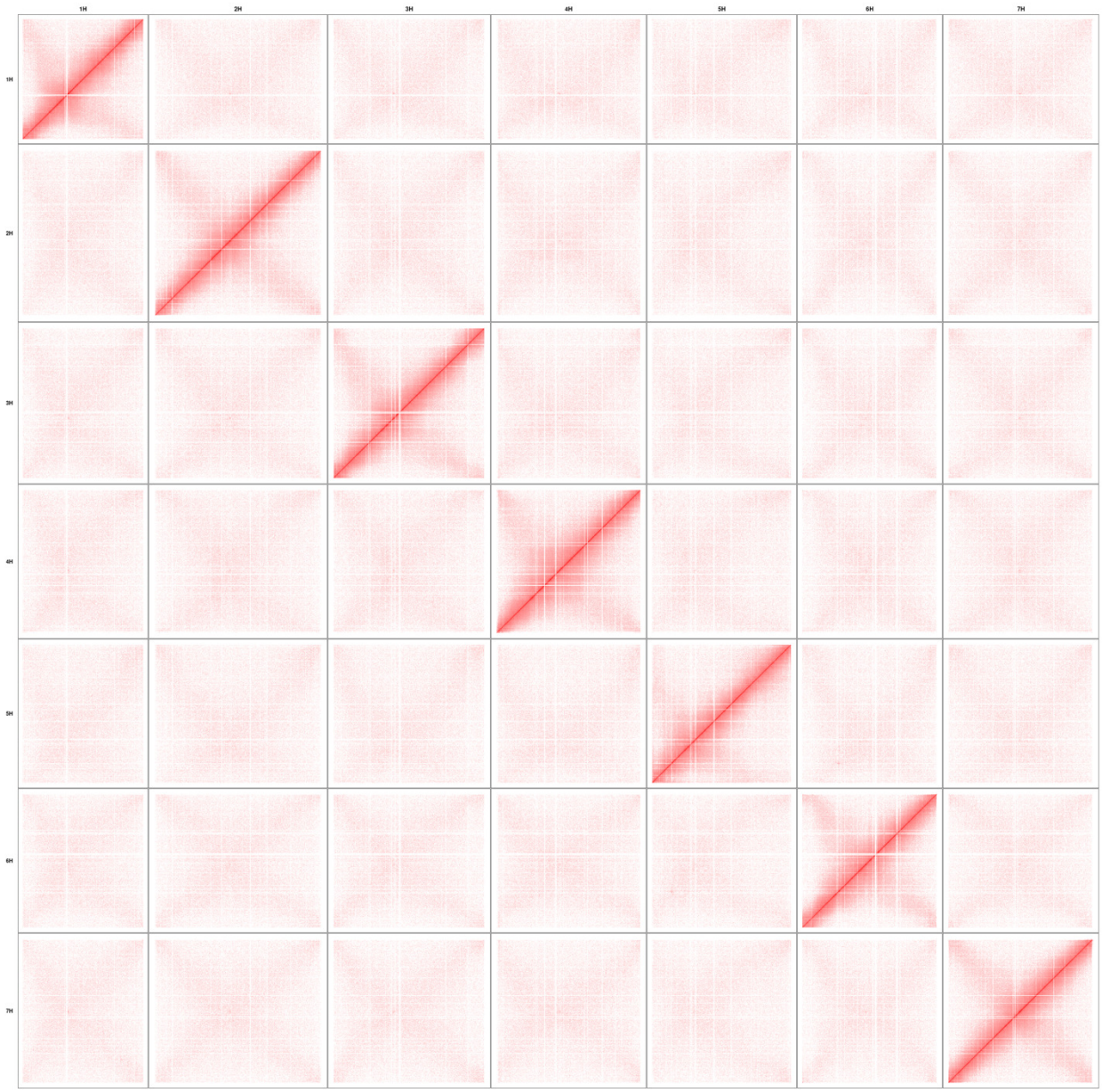

Supplementary Figure 4: *H. chilense* GRA1000 Hi-C contact matrix. The intensity of pixels represents the normalized count of Hi-C links between 1 Mb windows on all chromosomes and haplotypes.

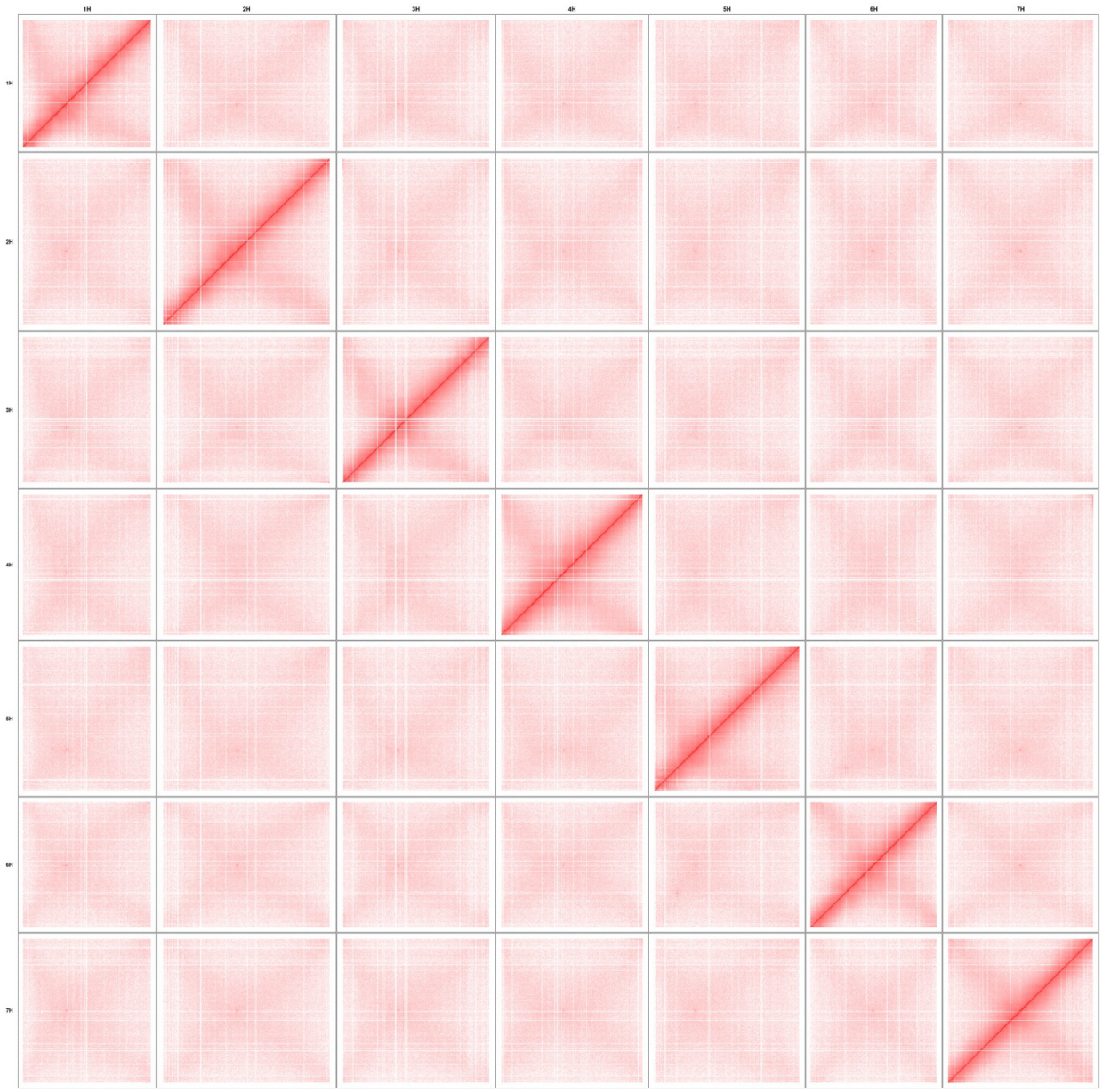

Supplementary Figure 5: *H. comosum* NGB18417 Hi-C contact matrix. The intensity of pixels represents the normalized count of Hi-C links between 1 Mb windows on all chromosomes and haplotypes.

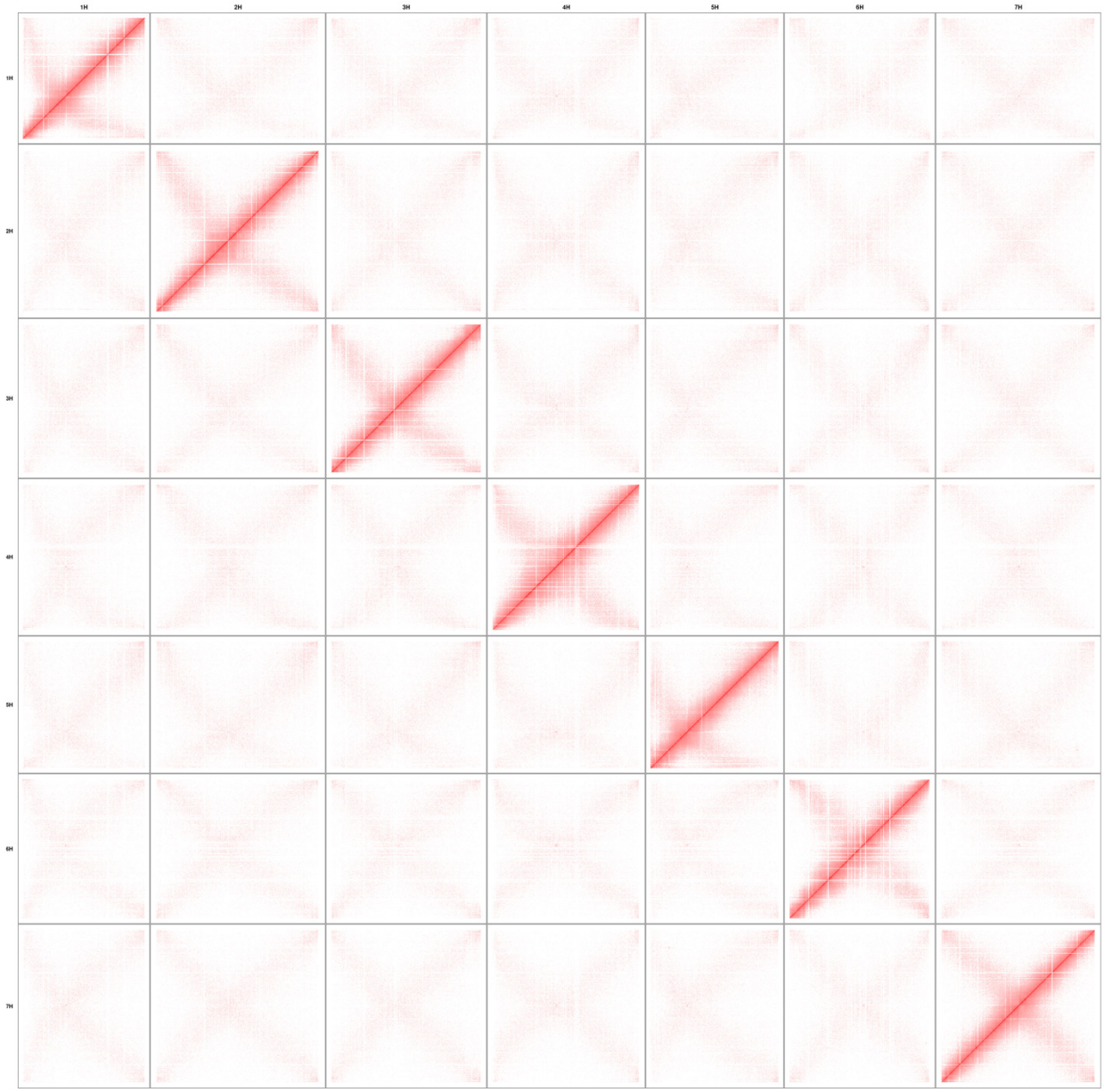

Supplementary Figure 6: *H. cordobense* BCC2067 Hi-C contact matrix. The intensity of pixels represents the normalized count of Hi-C links between 1 Mb windows on all chromosomes and haplotypes.

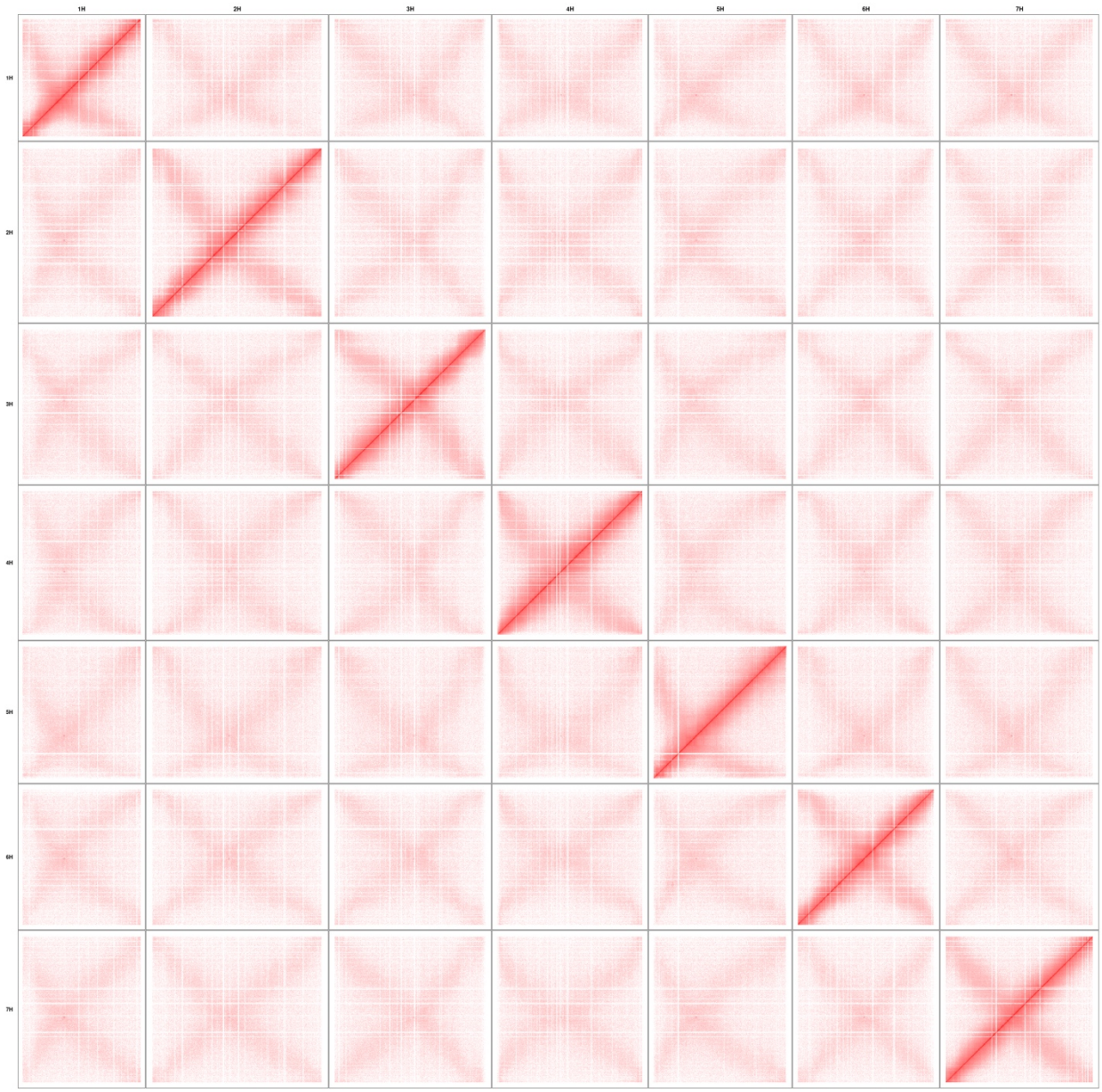

Supplementary Figure 7: *H. erectifolium* NGB6816 Hi-C contact matrix. The intensity of pixels represents the normalized count of Hi-C links between 1 Mb windows on all chromosomes and haplotypes.

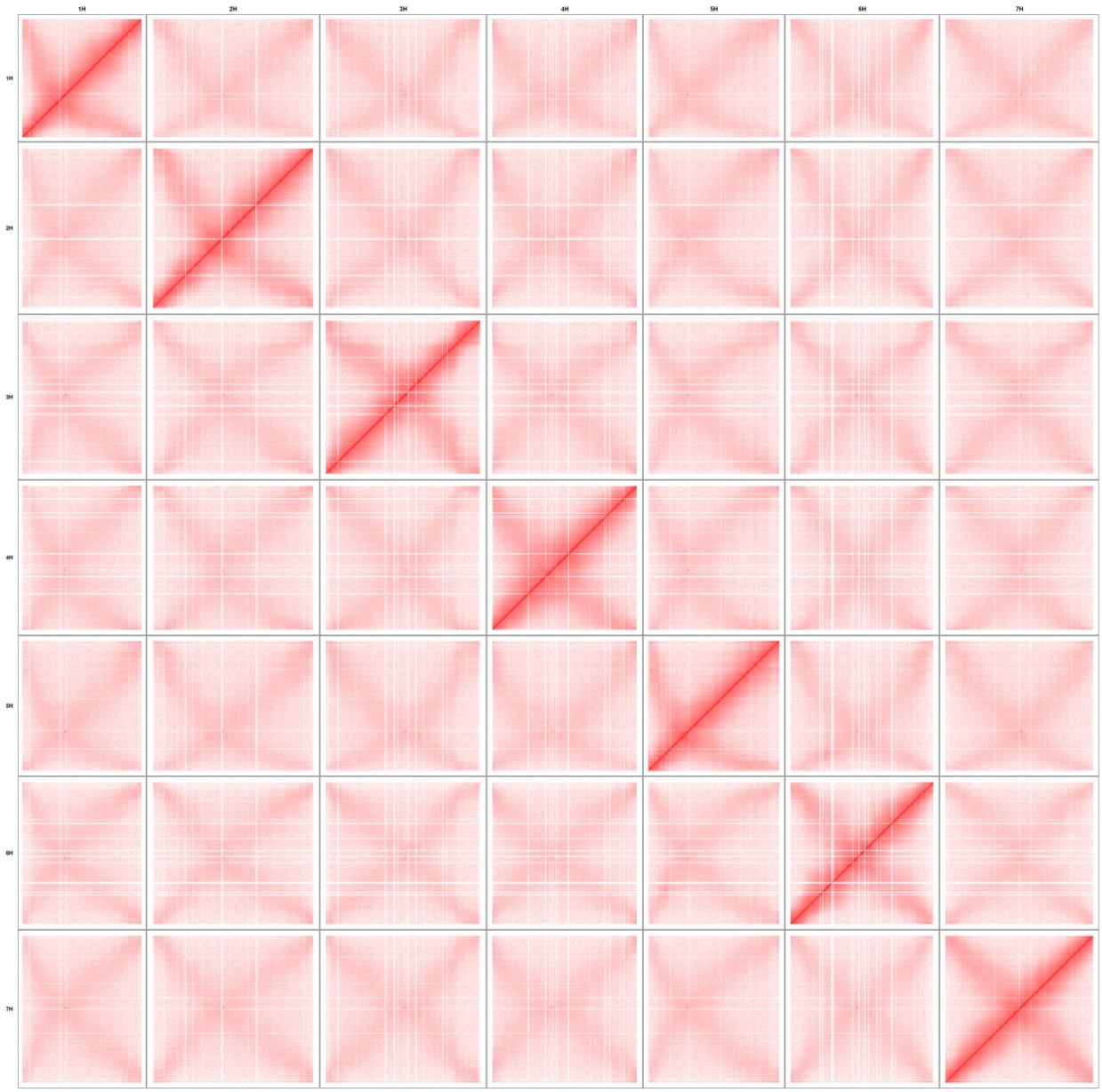

Supplementary Figure 8: *H. euclaston* NGB90233 Hi-C contact matrix. The intensity of pixels represents the normalized count of Hi-C links between 1 Mb windows on all chromosomes and haplotypes.

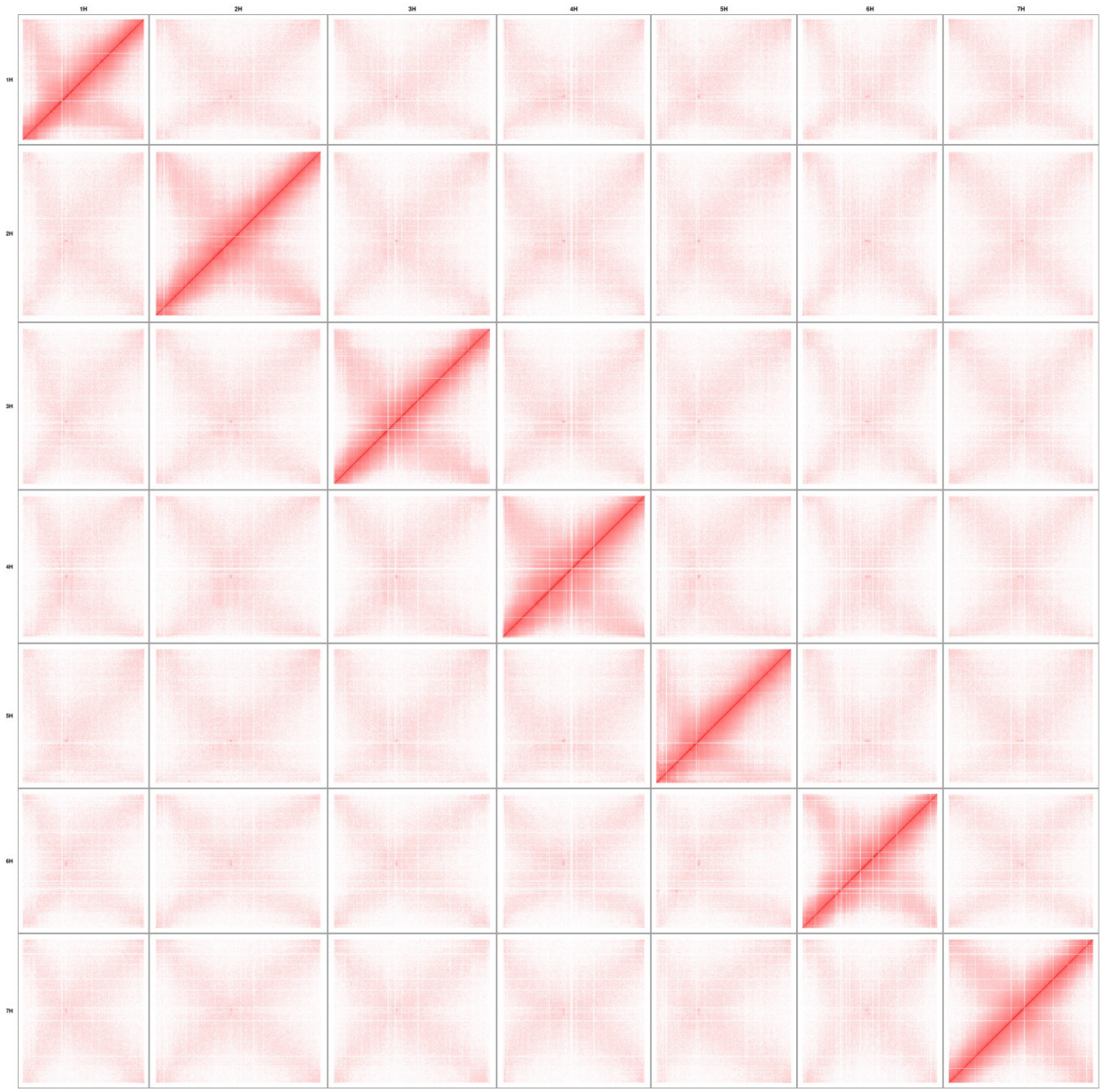

Supplementary Figure 9: *H. flexuosum* BCC2023 Hi-C contact matrix. The intensity of pixels represents the normalized count of Hi-C links between 1 Mb windows on all chromosomes and haplotypes.

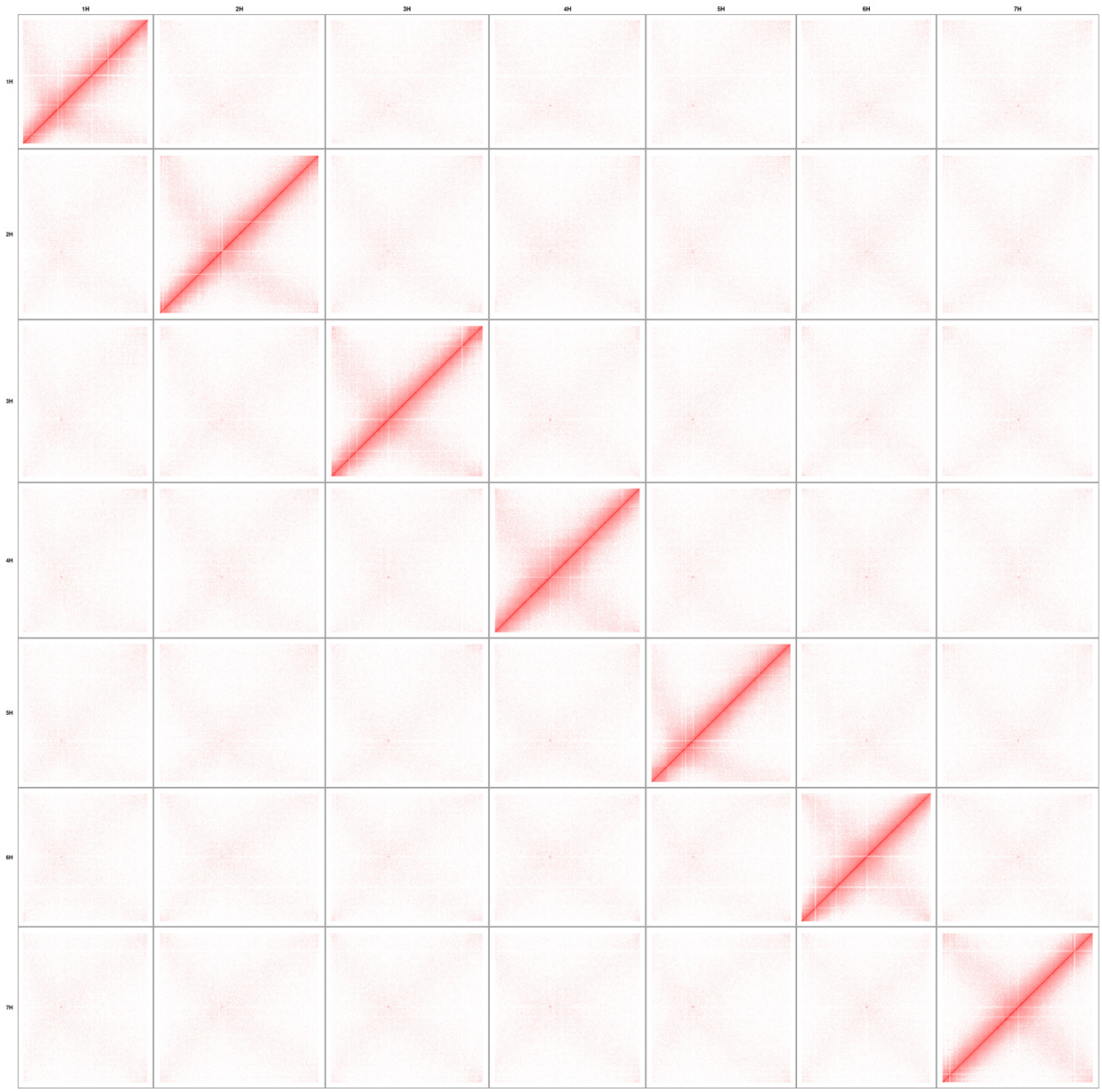

Supplementary Figure 10: *H. gussoneanum* BCC2005 Hi-C contact matrix. The intensity of pixels represents the normalized count of Hi-C links between 1 Mb windows on all chromosomes and haplotypes.

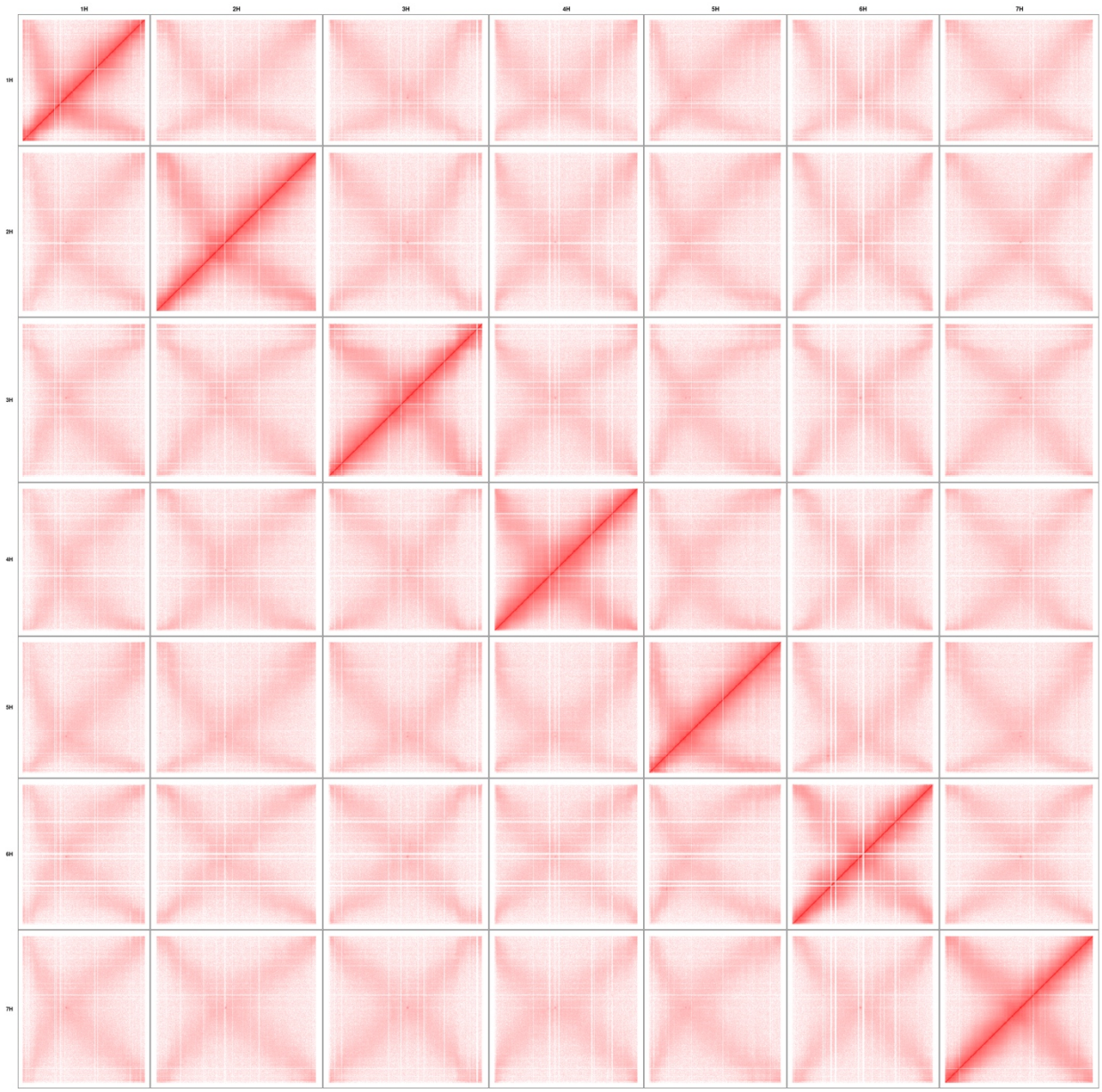

Supplementary Figure 11: *H. intercedens* NGB15676 Hi-C contact matrix. The intensity of pixels represents the normalized count of Hi-C links between 1 Mb windows on all chromosomes and haplotypes.

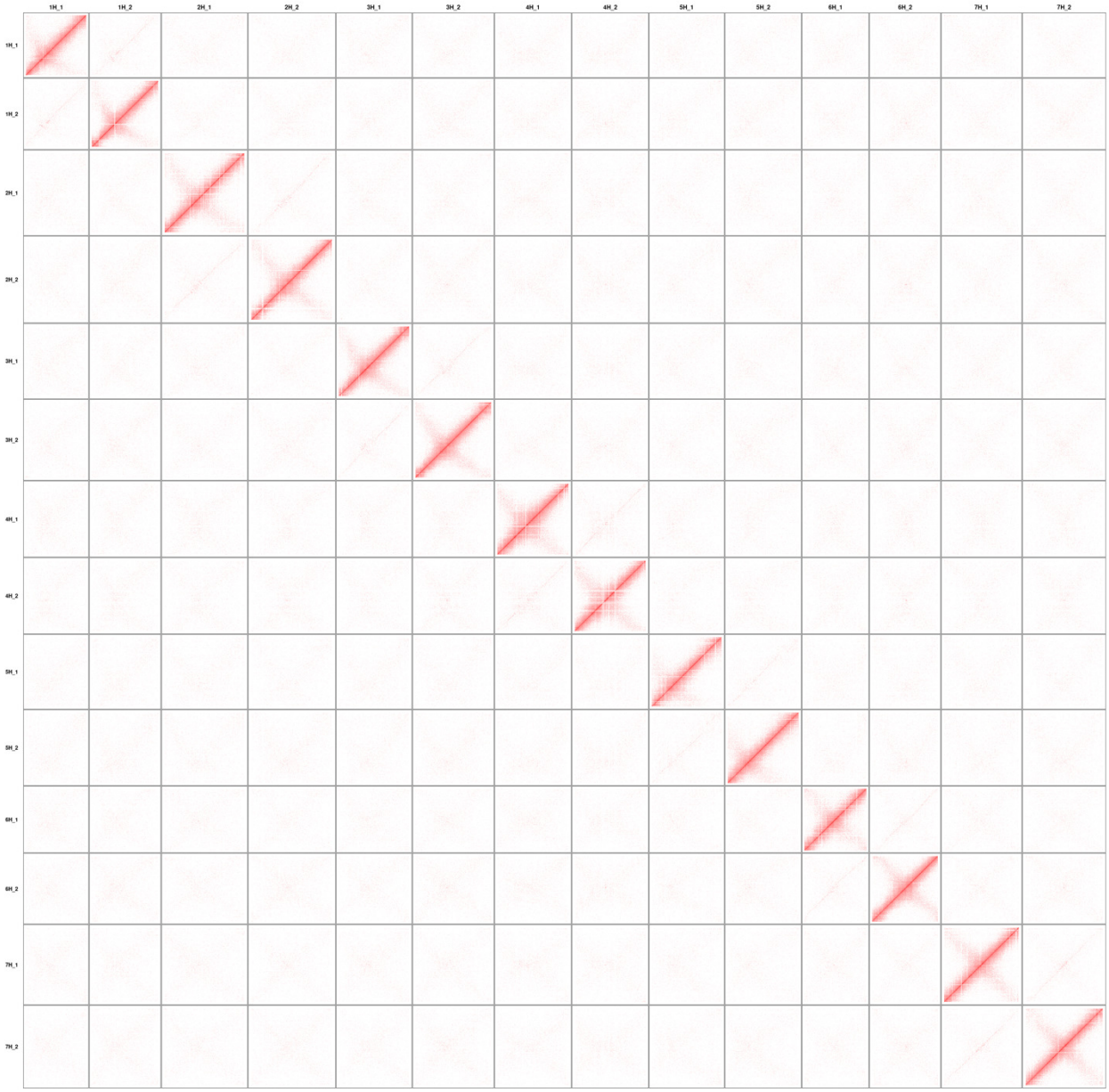

Supplementary Figure 12: *H. jubatum* BCC2055 Hi-C contact matrix. The intensity of pixels represents the normalized count of Hi-C links between 1 Mb windows on all chromosomes and haplotypes.

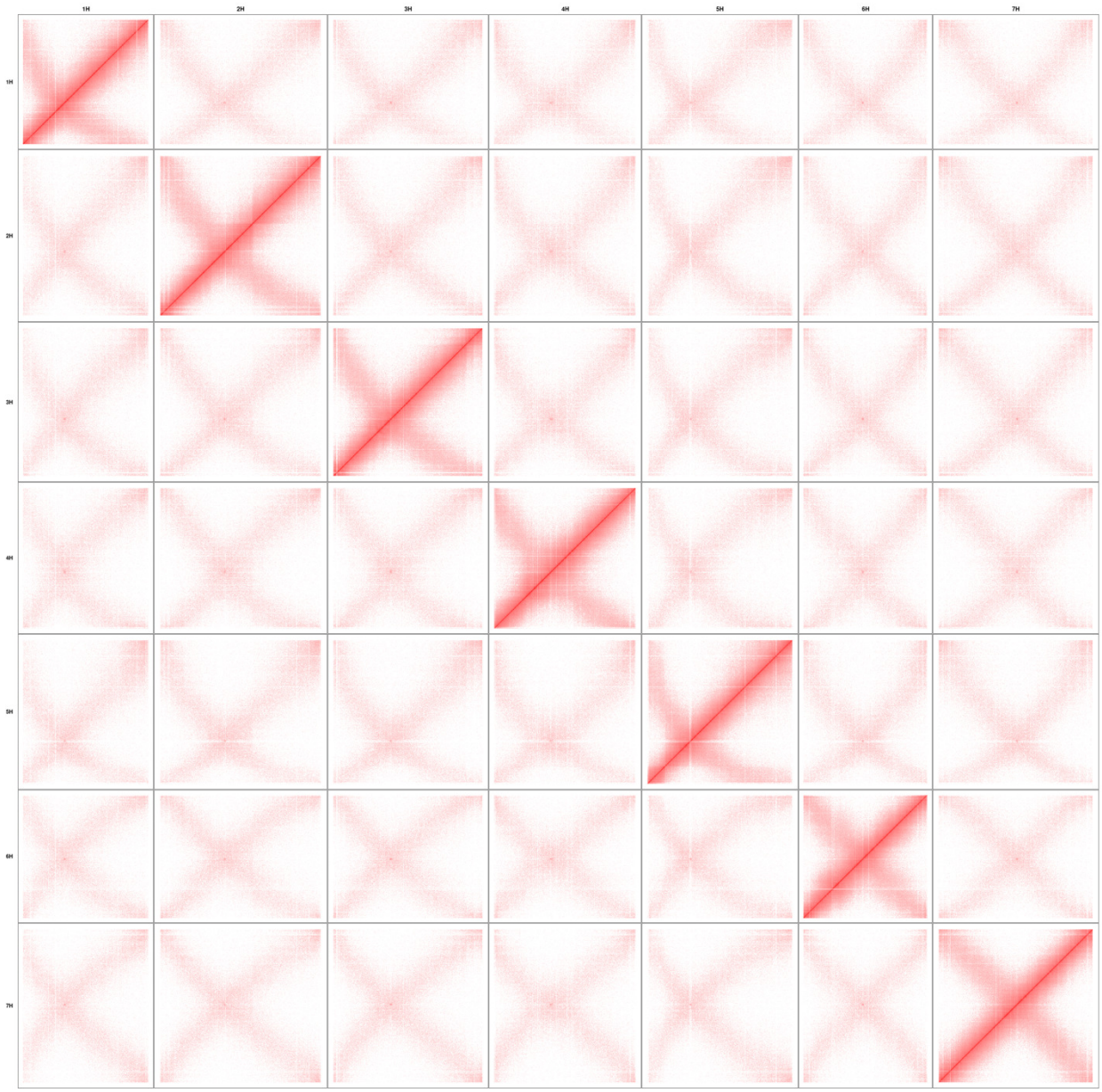

Supplementary Figure 13: *H. marinum* BCC2001 Hi-C contact matrix. The intensity of pixels represents the normalized count of Hi-C links between 1 Mb windows on all chromosomes and haplotypes.

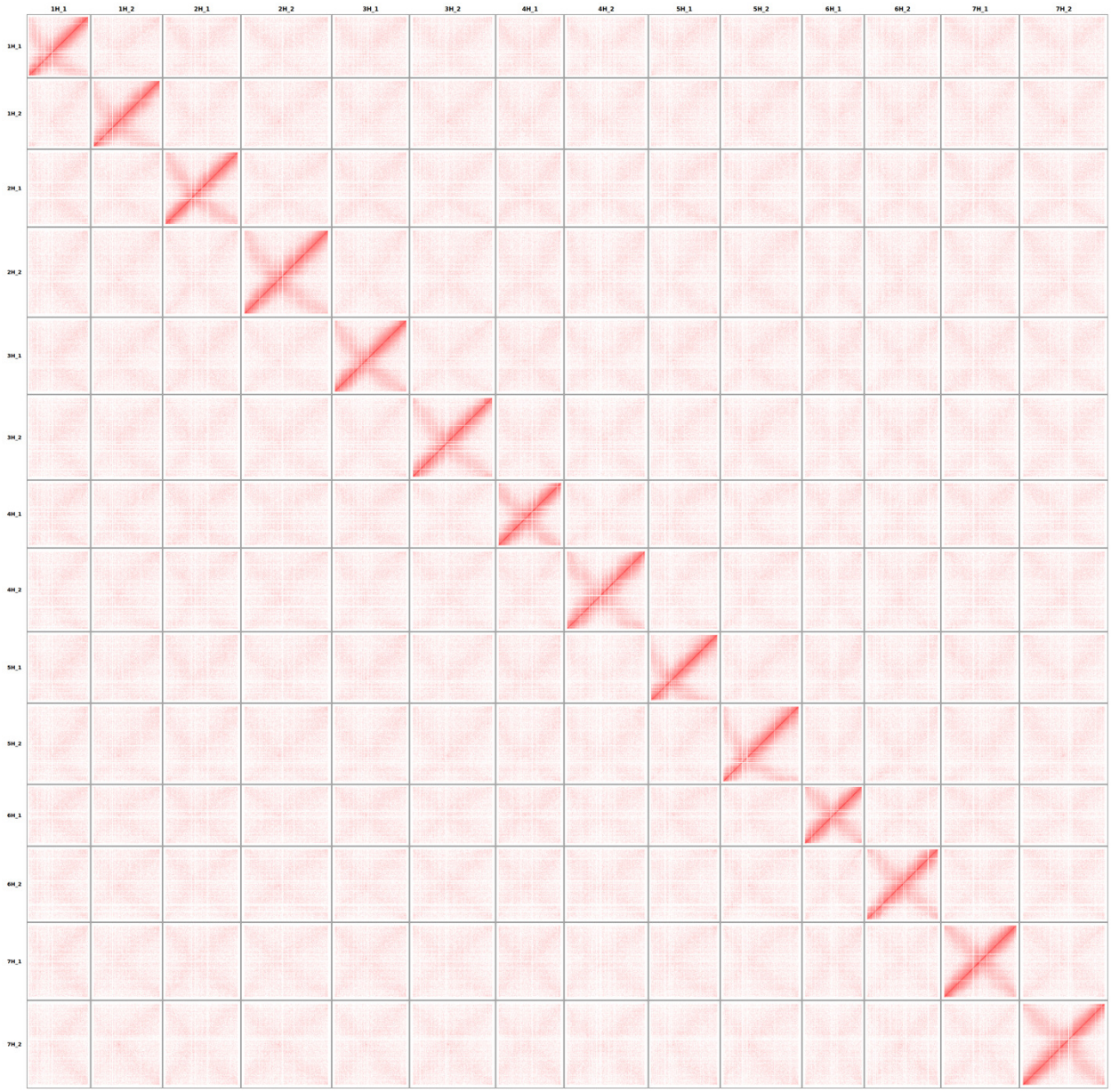

Supplementary Figure 14: *H. murinum* BCC2009 Hi-C contact matrix. The intensity of pixels represents the normalized count of Hi-C links between 1 Mb windows on all chromosomes and haplotypes.

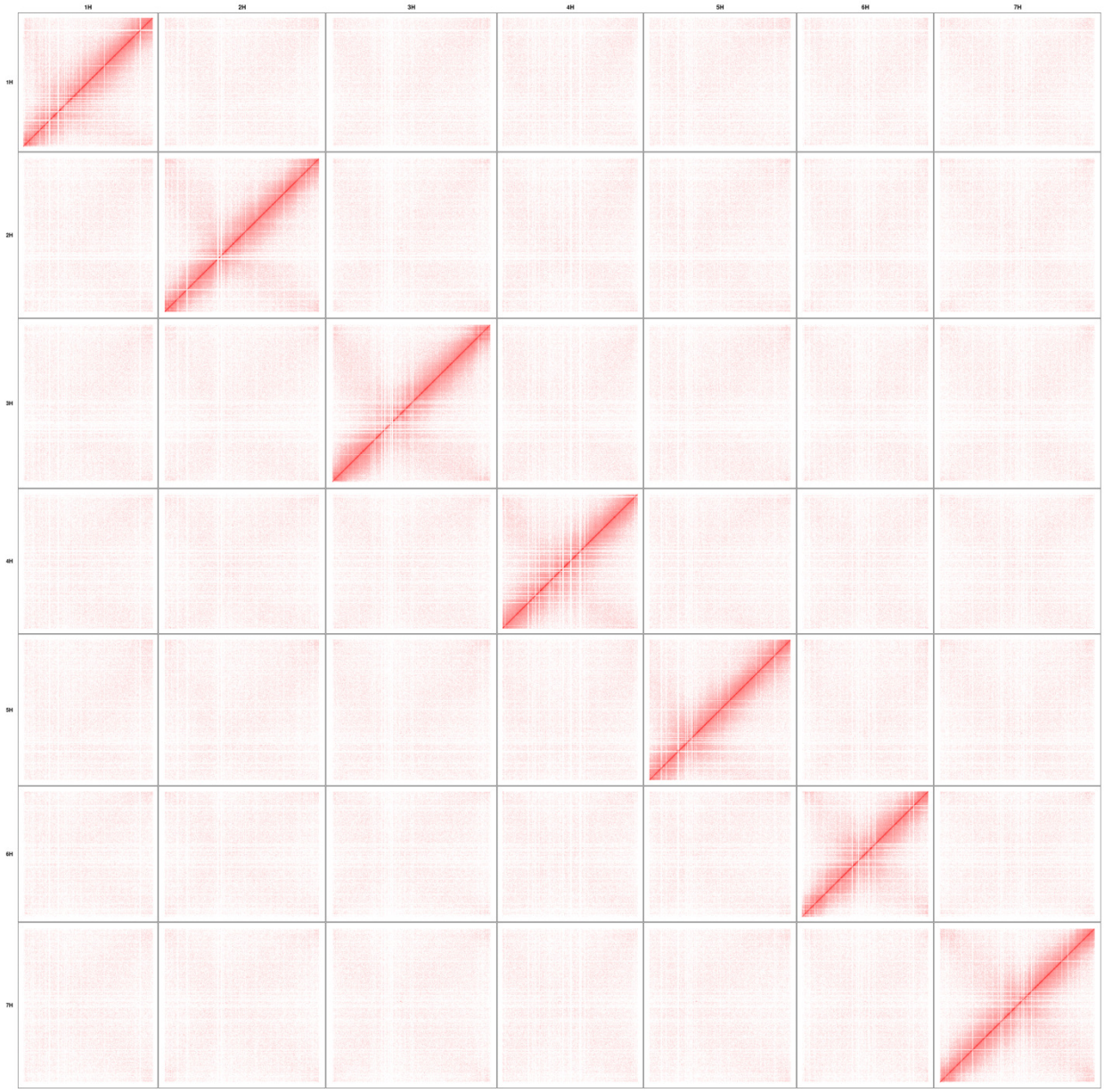

Supplementary Figure 15: *H. murinum* BCC2017 Hi-C contact matrix. The intensity of pixels represents the normalized count of Hi-C links between 1 Mb windows on all chromosomes and haplotypes.

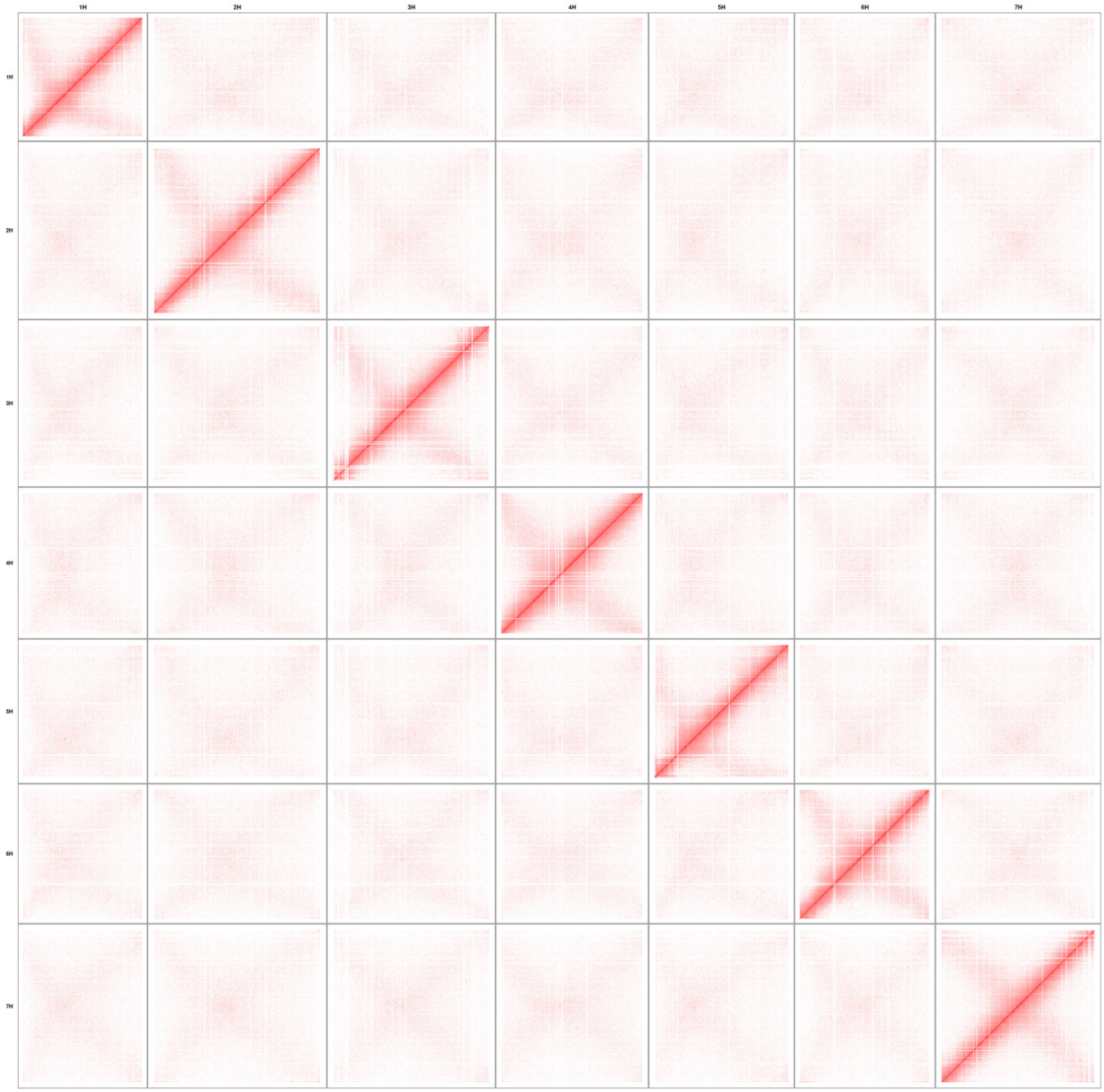

Supplementary Figure 16: *H. muticum* NGB90062 Hi-C contact matrix. The intensity of pixels represents the normalized count of Hi-C links between 1 Mb windows on all chromosomes and haplotypes.

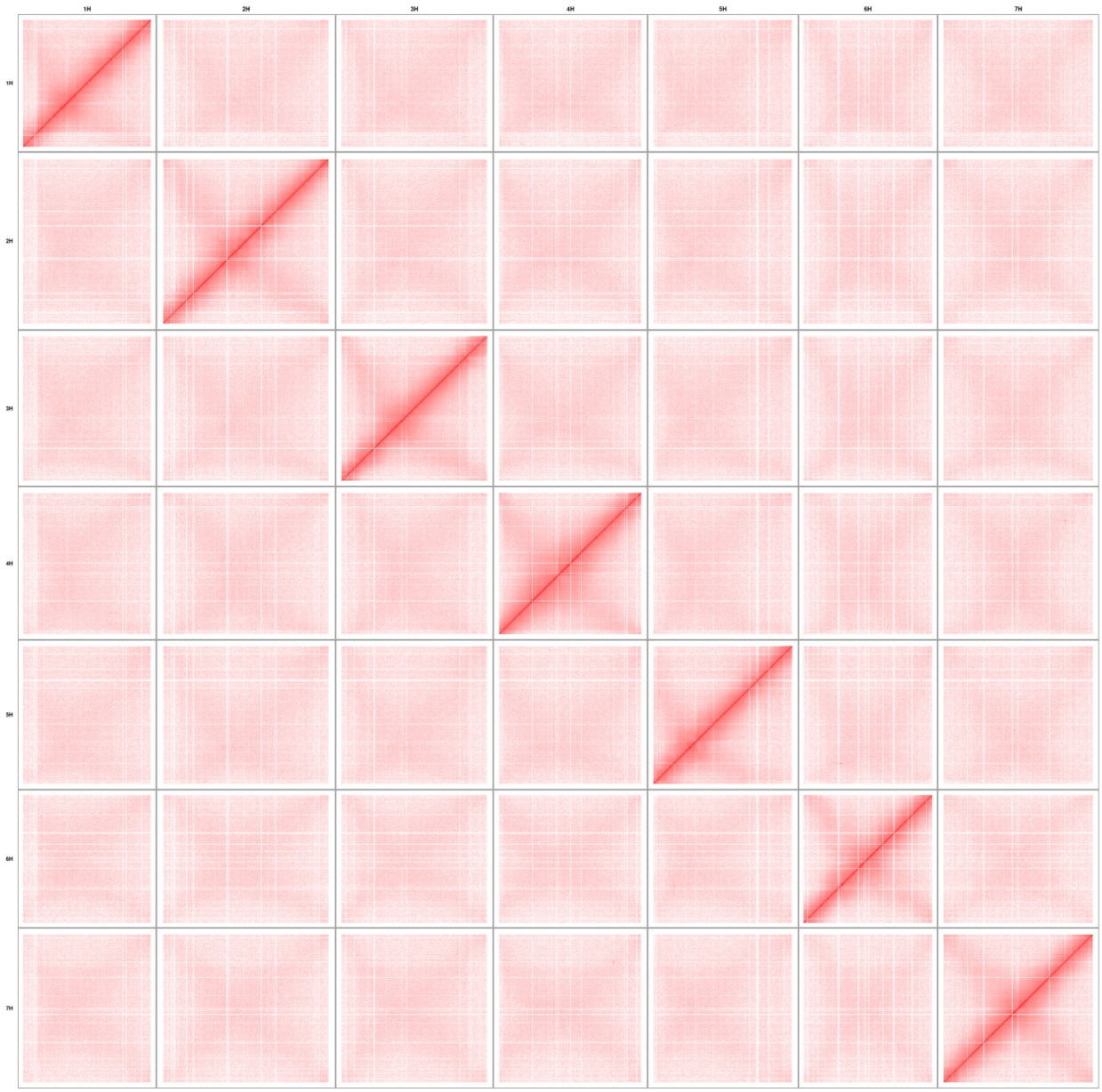

Supplementary Figure 17: *H. patagonicum* BCC2065 Hi-C contact matrix. The intensity of pixels represents the normalized count of Hi-C links between 1 Mb windows on all chromosomes and haplotypes.

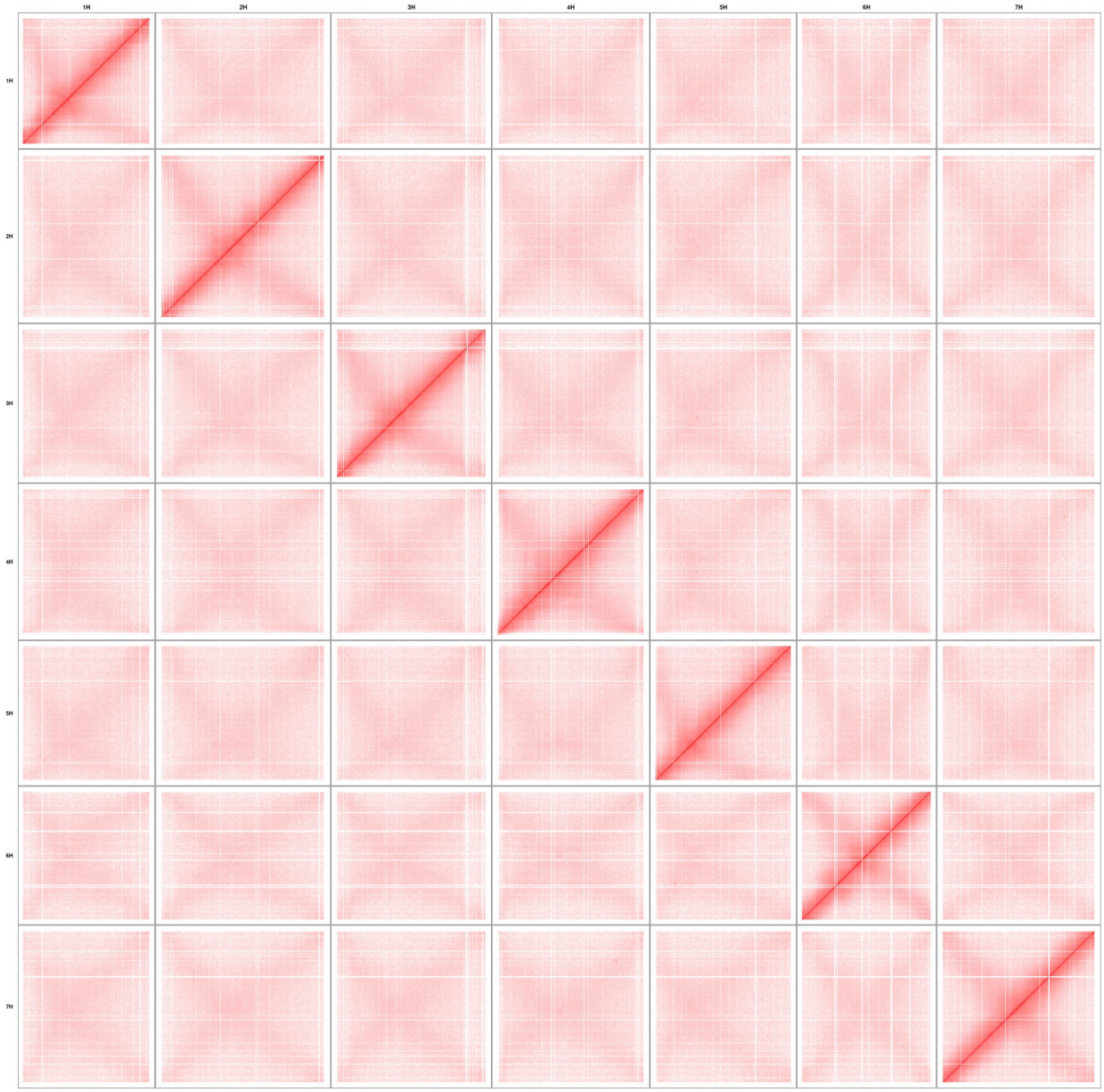

Supplementary Figure 18: *H. pubiflorum* BCC2028 Hi-C contact matrix. The intensity of pixels represents the normalized count of Hi-C links between 1 Mb windows on all chromosomes and haplotypes.

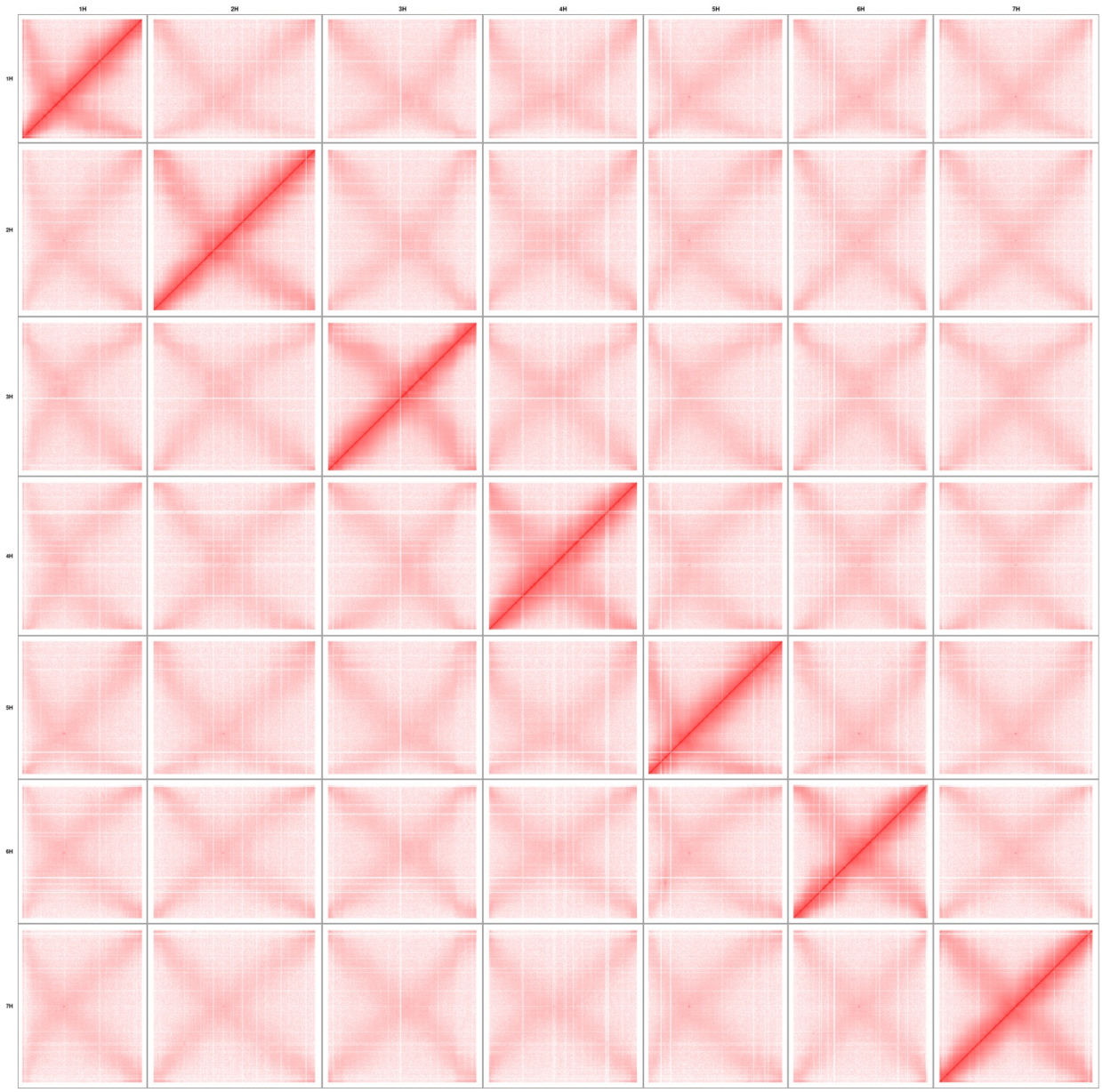

Supplementary Figure 19: *H. pusillum* NGB6888 Hi-C contact matrix. The intensity of pixels represents the normalized count of Hi-C links between 1 Mb windows on all chromosomes and haplotypes.

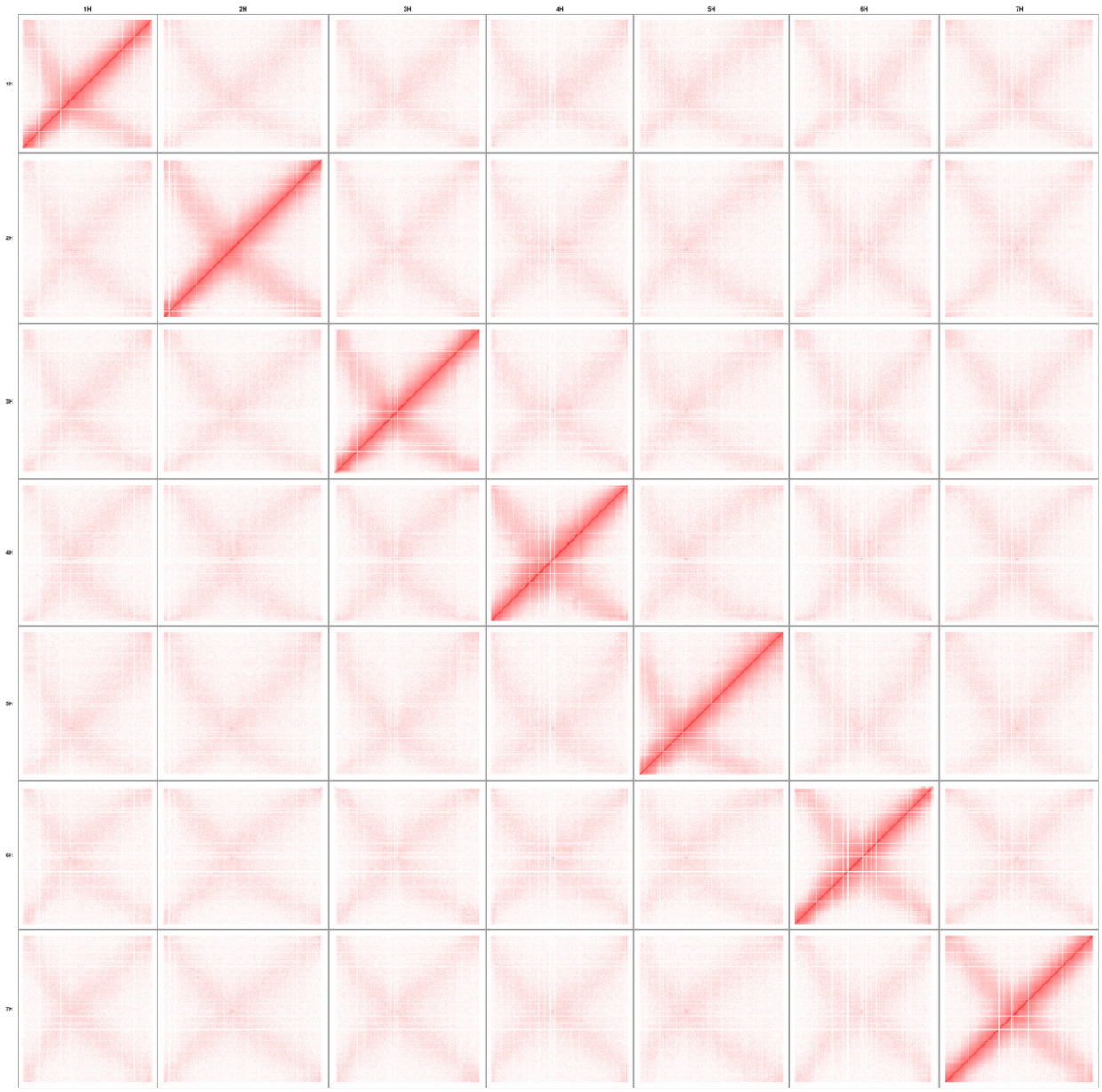

Supplementary Figure 20: *H. roshevitzii* BCC2069 Hi-C contact matrix. The intensity of pixels represents the normalized count of Hi-C links between 1 Mb windows on all chromosomes and haplotypes.

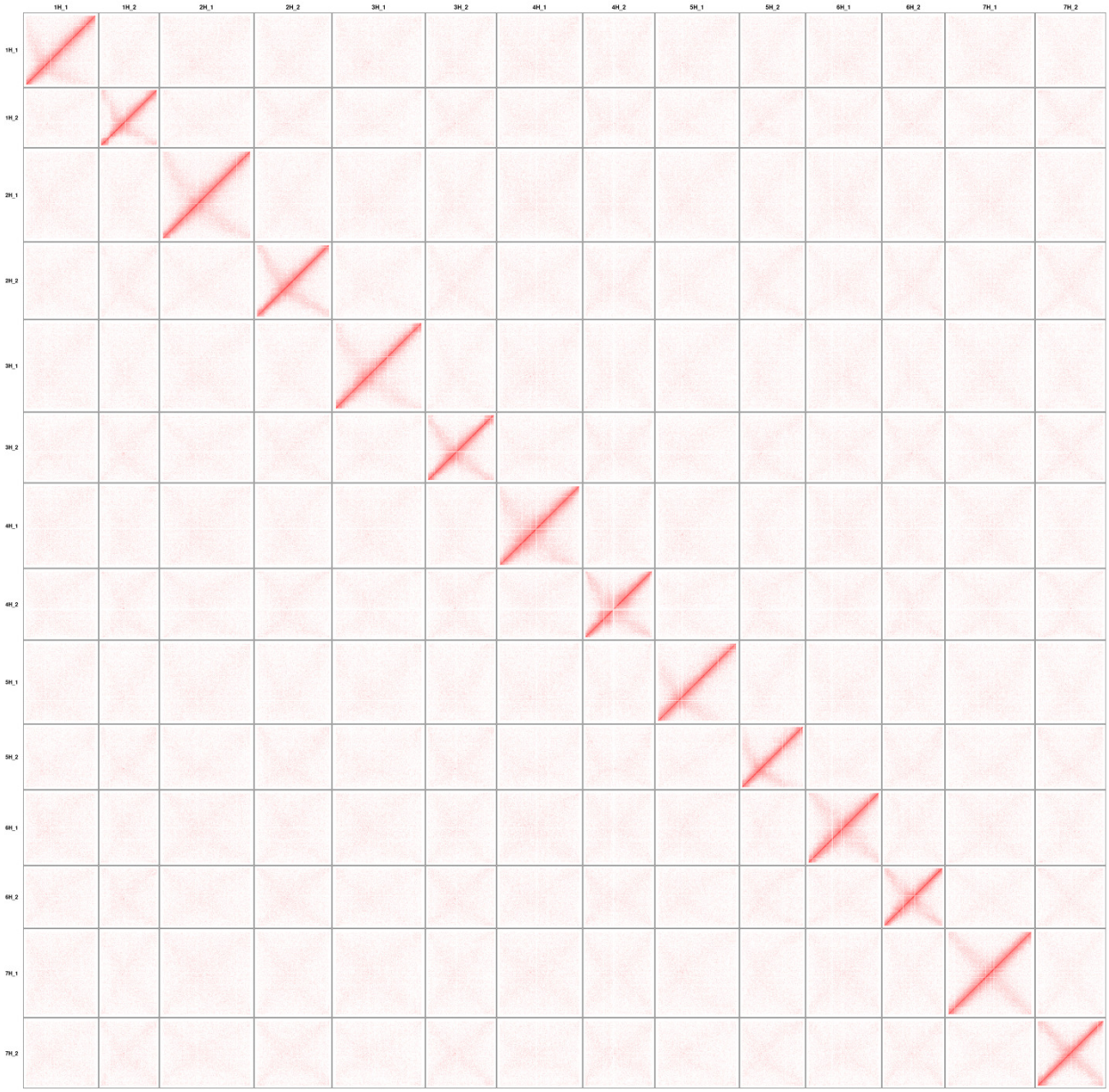

Supplementary Figure 21: *H. secalinum* BCC2004 Hi-C contact matrix. The intensity of pixels represents the normalized count of Hi-C links between 1 Mb windows on all chromosomes and haplotypes.

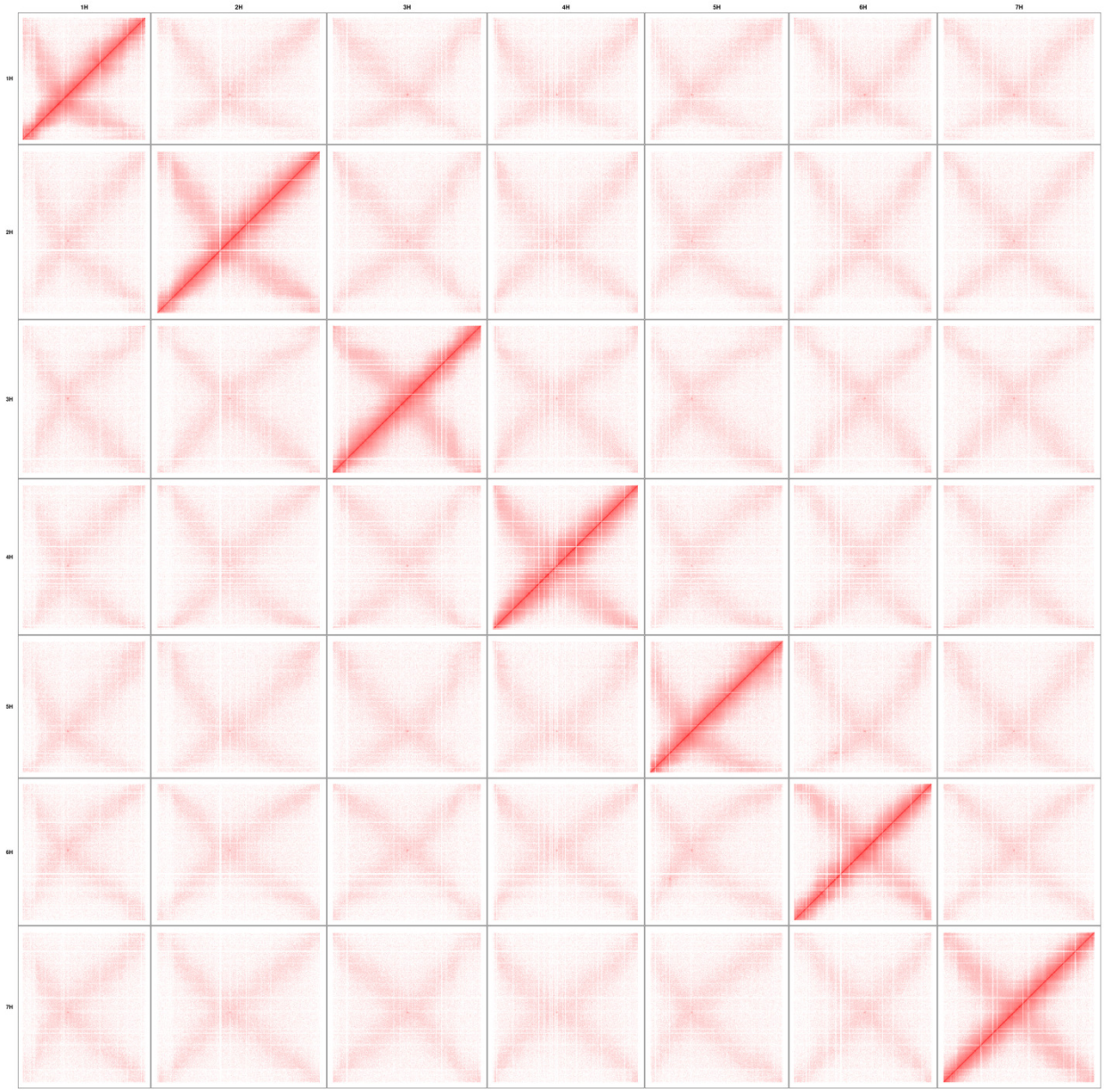

Supplementary Figure 22: *H. stenostachys* NGB90152 Hi-C contact matrix. The intensity of pixels represents the normalized count of Hi-C links between 1 Mb windows on all chromosomes and haplotypes.

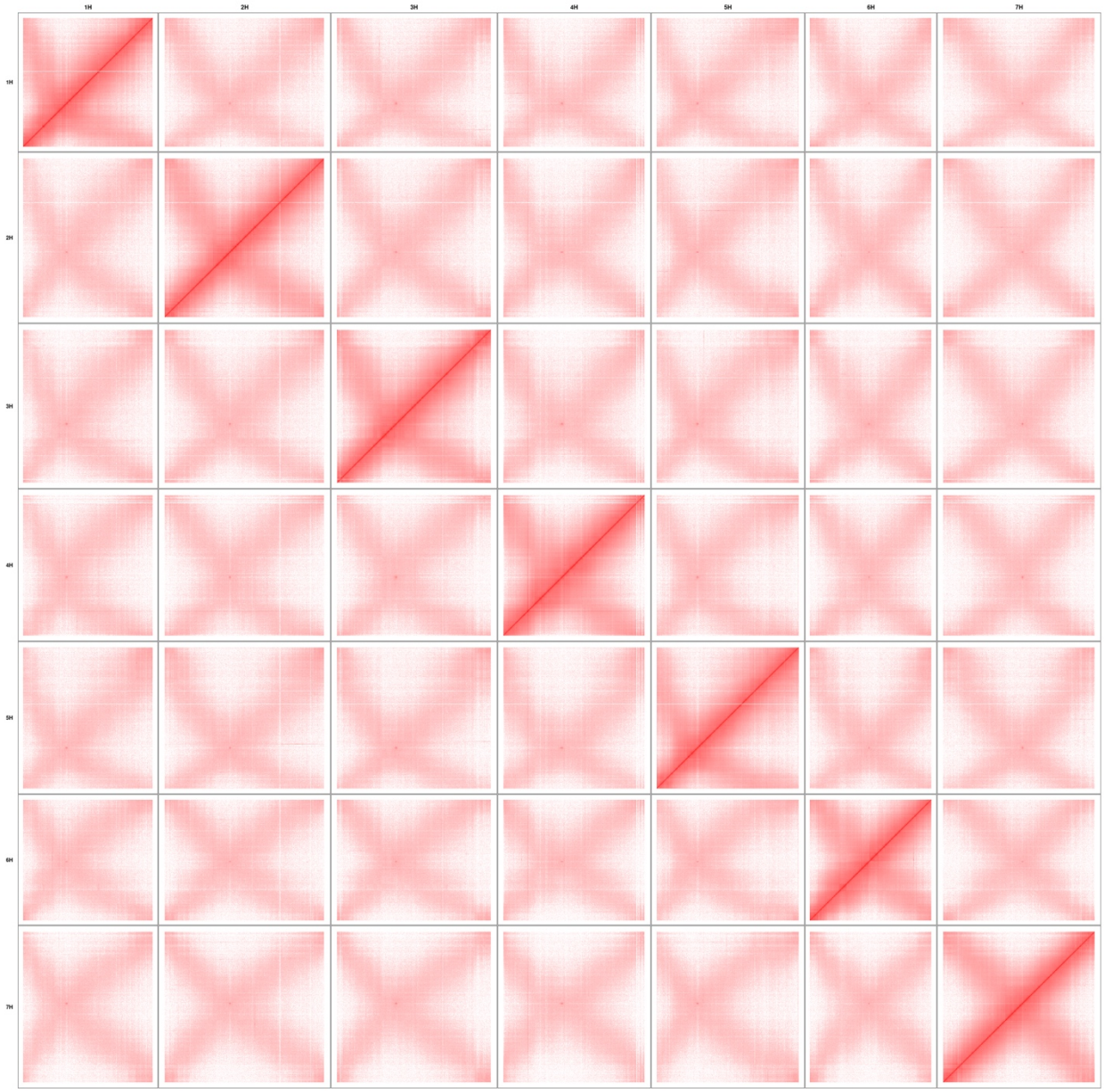

Supplementary Figure 23: *H. marinum* H559 Hi-C contact matrix. The intensity of pixels represents the normalized count of Hi-C links between 1 Mb windows on all chromosomes and haplotypes.

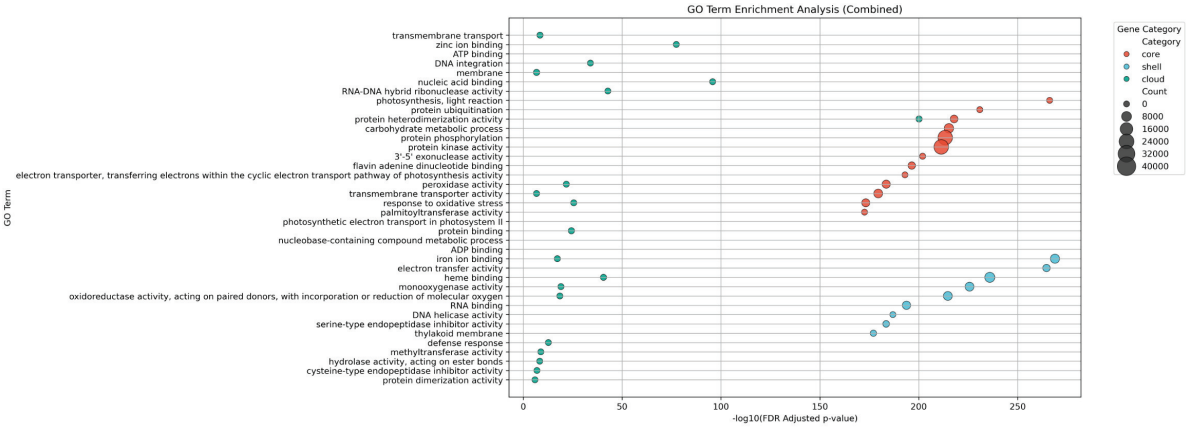

Supplementary Figure 24: GO-term enrichment for core, shell and cloud genes visualised by bubble plots.

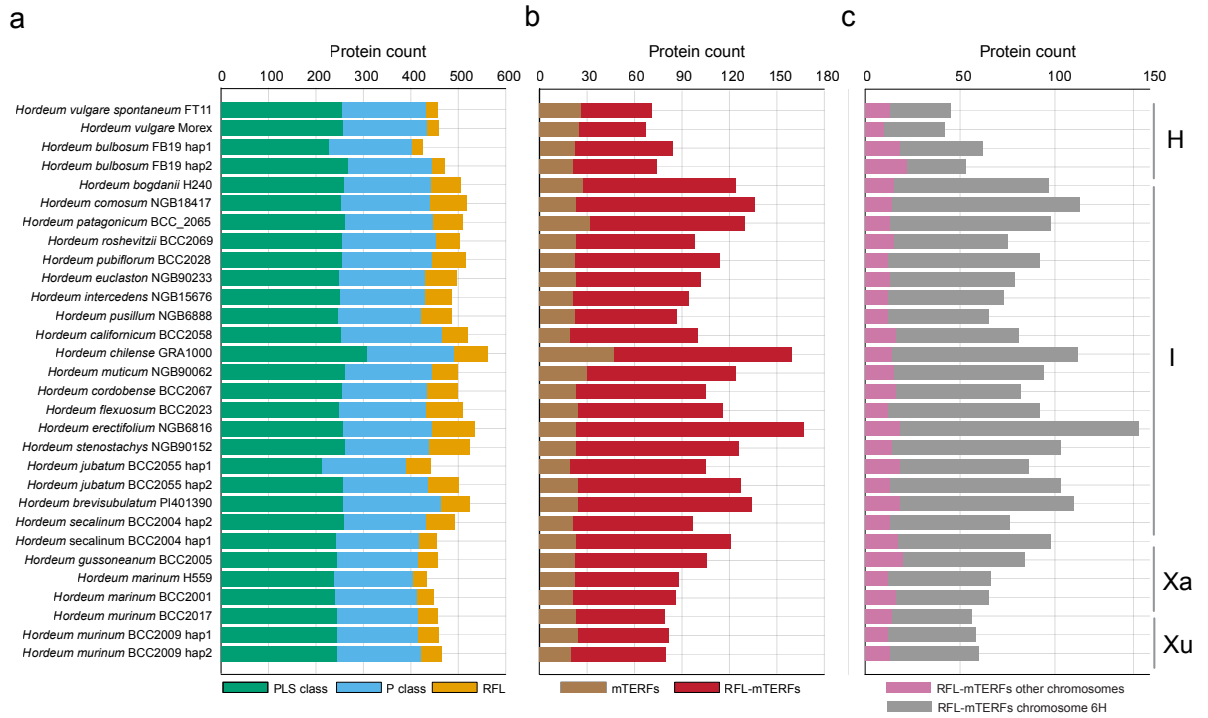
a
b
c
Protein count
0 100 200 300 400 500 600
0 30 60 90 120 150 180
0 50 100 150
Hordeum vulgare spontaneum FT11
Hordeum vulgare Morex
Hordeum bulbosum FB19 hap1
Hordeum bulbosum FB19 hap2
Hordeum bogdanii H240
Hordeum comosum NGB18417
Hordeum patagonicum BCC_2065
Hordeum roshevitzii BCC2069
Hordeum pubiflorum BCC2028
Hordeum euclaston NGB90233
Hordeum intercedens NGB15676
Hordeum pusillum NGB6888
Hordeum californicum BCC2058
Hordeum chilense GRA1000
Hordeum muticum NGB90062
Hordeum cordobense BCC2067
Hordeum flexuosum BCC2023
Hordeum erectifolium NGB6816
Hordeum stenostachys NGB90152
Hordeum jubatum BCC2055 hap1
Hordeum jubatum BCC2055 hap2
Hordeum brevisubulatum PI401390
Hordeum secalinum BCC2004 hap2
Hordeum secalinum BCC2004 hap1
Hordeum gussoneanum BCC2005
Hordeum marinum H559
Hordeum marinum BCC2001
Hordeum murinum BCC2017
Hordeum murinum BCC2009 hap1
Hordeum murinum BCC2009 hap2
H
I
Xa
Xu
PLS class
P class
RFL
mTERFs
RFL-mTERFs
RFL-mTERFs other chromosomes
RFL-mTERFs chromosome 6H

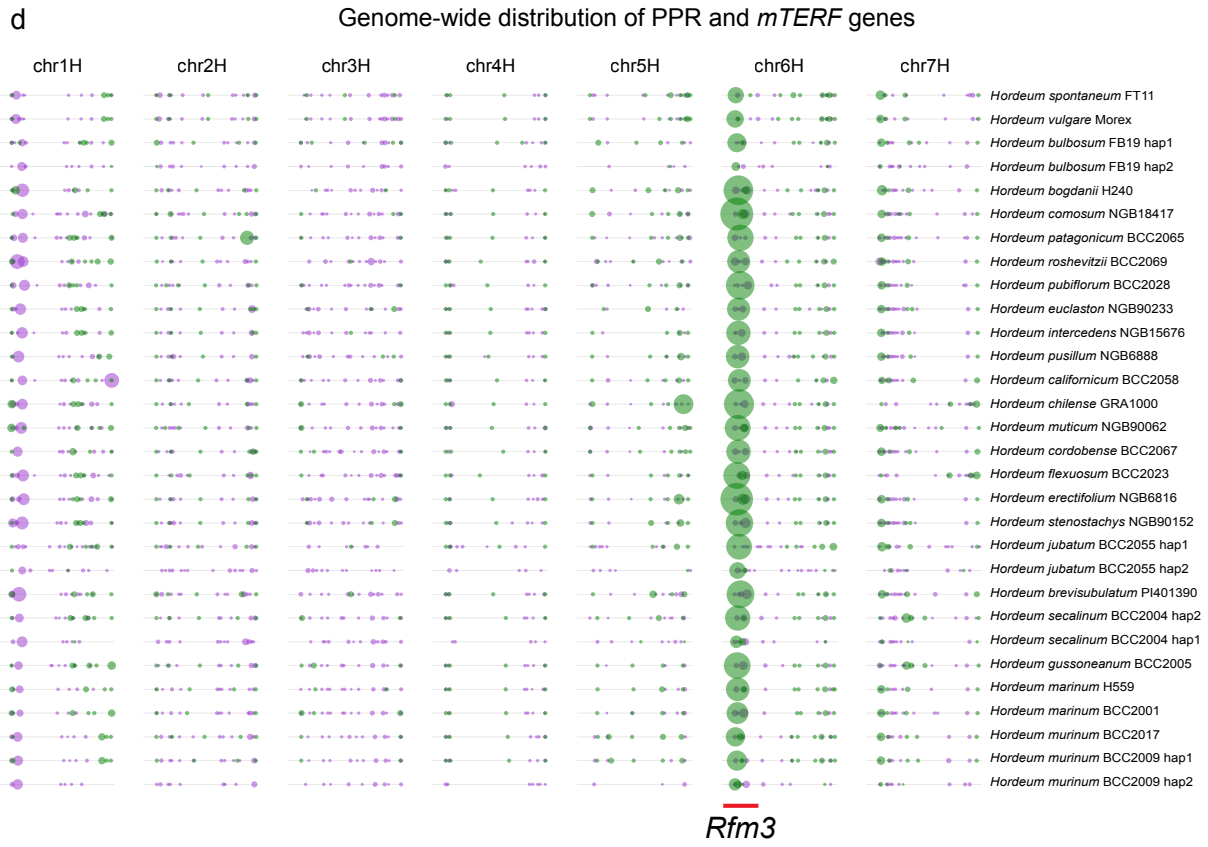
d
Genome-wide distribution of PPR and mTERF genes
chr1H
chr2H
chr3H
chr4H
chr5H
chr6H
chr7H
Hordeum spontaneum FT11
Hordeum vulgare Morex
Hordeum bulbosum FB19 hap1
Hordeum bulbosum FB19 hap2
Hordeum bogdanii H240
Hordeum comosum NGB18417
Hordeum patagonicum BCC2065
Hordeum roshevitzii BCC2069
Hordeum pubiflorum BCC2028
Hordeum euclaston NGB90233
Hordeum intercedens NGB15676
Hordeum pusillum NGB6888
Hordeum californicum BCC2058
Hordeum chilense GRA1000
Hordeum muticum NGB90062
Hordeum cordobense BCC2067
Hordeum flexuosum BCC2023
Hordeum erectifolium NGB6816
Hordeum stenostachys NGB90152
Hordeum jubatum BCC2055 hap1
Hordeum jubatum BCC2055 hap2
Hordeum brevisubulatum PI401390
Hordeum secalinum BCC2004 hap2
Hordeum secalinum BCC2004 hap1
Hordeum gussoneanum BCC2005
Hordeum marinum H559
Hordeum marinum BCC2001
Hordeum murinum BCC2017
Hordeum murinum BCC2009 hap1
Hordeum murinum BCC2009 hap2
Rfm3

Supplementary Figure 25. Pangenome analyses of the PPR and mTERF gene families in *Hordeum*. **(a)** Copy number variation of the PLS, P and RFL-type PPR proteins. The genes were identified using the PPRfinder software (https://github.com/ian-small/PPRfinder). **(b)** Copy number variation of the mTERF and RFL-mTERF genes. While the number of non-RFL mTERF genes remains consistent across species, the number of RFL-type mTERF genes varies substantially. Particularly high numbers of RFL-mTERFs are seen in genome group I. The mTERF sequences were identified using the Pfam domain PF02536. **(c)** The variation in the size of the RFL-mTERF clade occurs mainly in the largest cluster on the short arm of chromosome 6H. **(d)** P-class PPR and mTERF gene density across the *Hordeum* genomes. The densest (and largest) clusters are found respectively on chr1H and chr6H, with juxtaposition of PPR and mTERF clusters on chr6H. PPR gene density is shown in purple, mTERF gene density in green. All positions are relative to chromosome length, i.e. all chromosomal x-axes range from 0 to 1. Circle areas are proportional to gene density calculated using a kernel density estimate. The genomic region carrying the *Rfm3* restorer gene locus is indicated by a red bar.

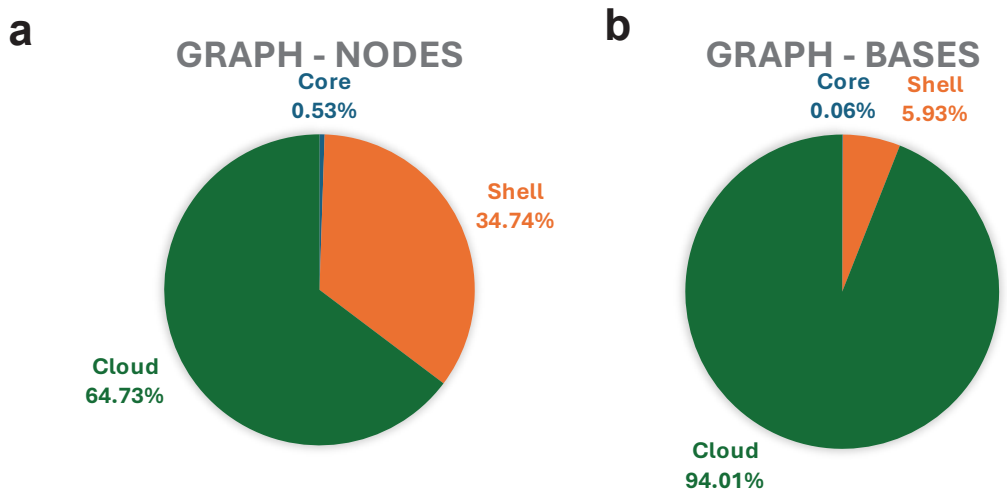

Supplementary Figure 26: Percentages of graph assigned to core (present in all accessions), shell (present in two or more but not all accessions) and cloud (present in a single accession only). (a) Node level assignment. **(b)** Base-level breakdown based on node membership shown in panel **(a)**. Membership was computed based on the number of accession paths visiting each node.

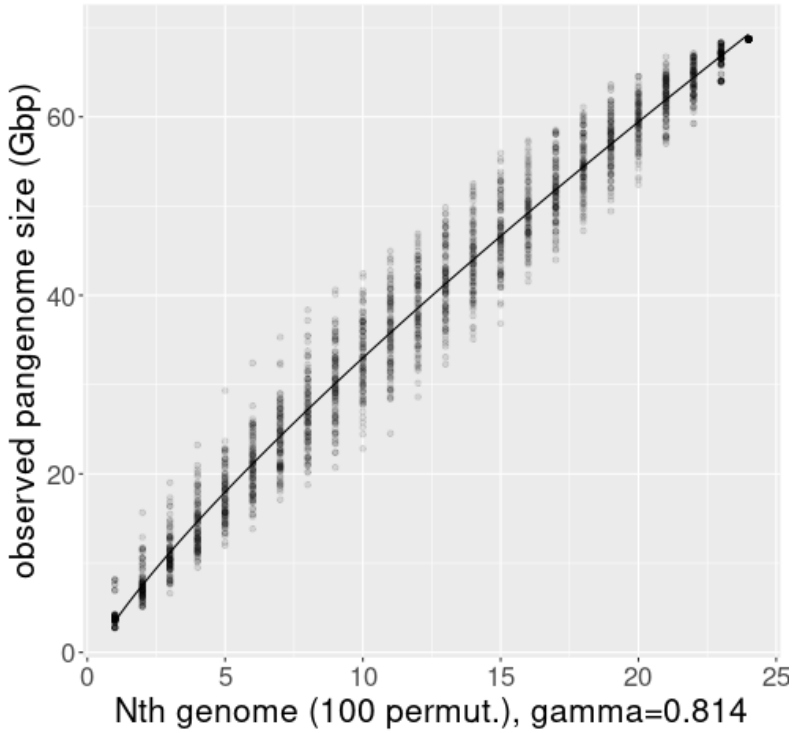

Supplementary Figure 27: Odgi heaps pan-genome saturation plot. The result shows total pangenome size as a function of the number of accessions added. One hundred permutations were computed for each number of accessions. The gamma coefficient of 0.8 indicates an open pan-genome, suggesting that not all of the variation in the genus has been captured. A gamma coefficient of < 0 indicates a closed pan-genome, whereas positive gamma values indicate an open pan-genome.

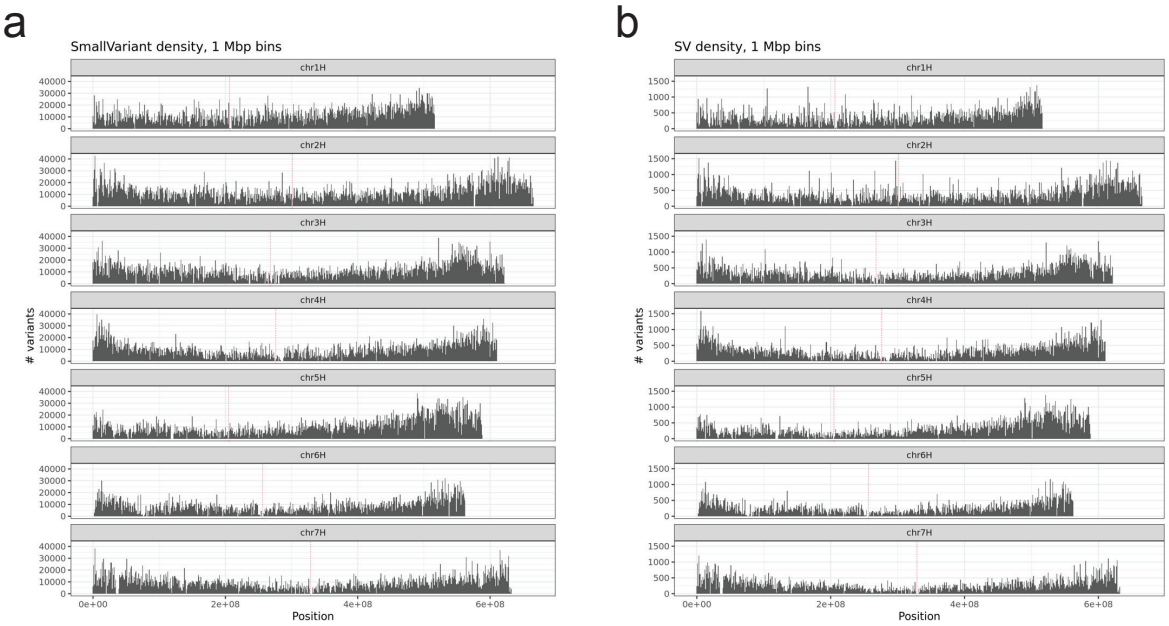

Supplementary Figure 28: Variant density as a function of position on the chromosome. The counts on the y-axis are the number of variants per 1 megabase bin. **(a)** Density of single nucleotide polymorphisms (SNPs). **(b)** Density of structural variants (> 50 basepair size). Red markers indicate position of centromeres. The breakdown of variants was 46,262,121 small variants versus 1,697,583 structural variants (insertions and deletions). Density of both SNPs and structural variants reflect patterns observed in other barley variant sets, with variant density generally increasing away from the pericentromeric regions where variation is suppressed due to a lack of recombination.

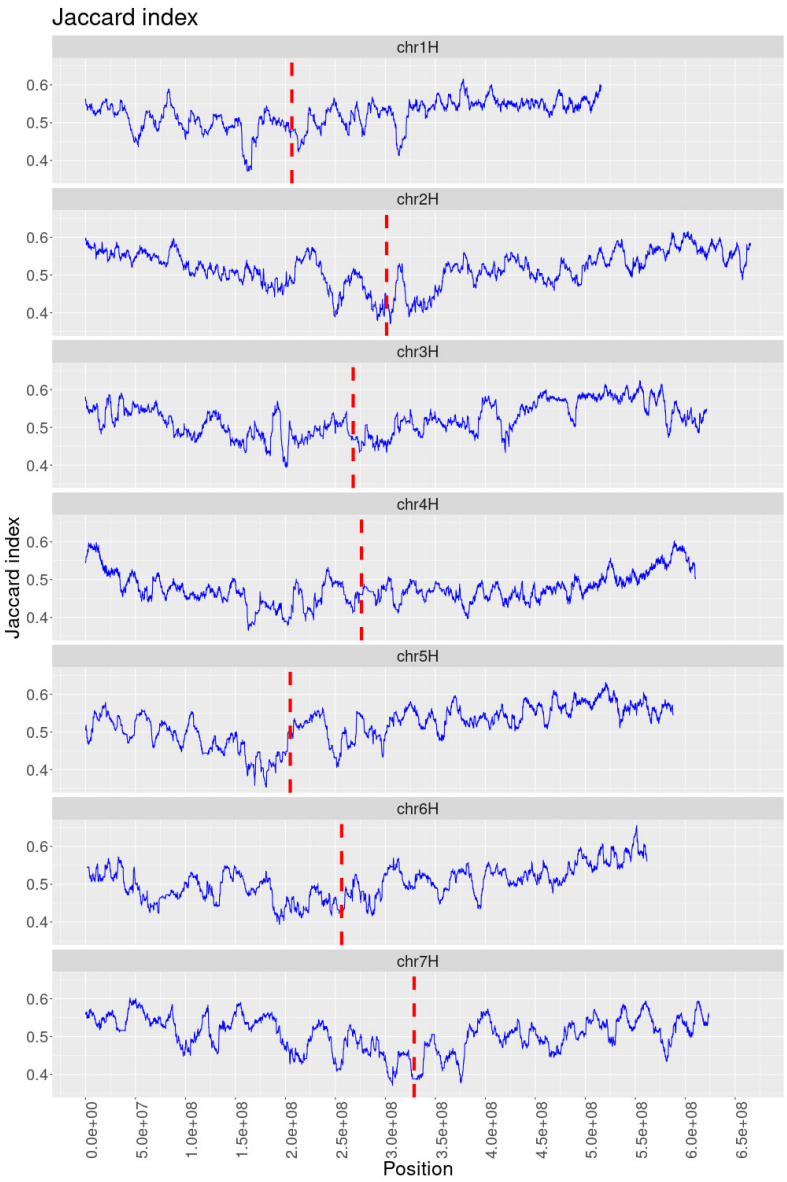

Supplementary Figure 29: Conservation analysis with *Pansel*. Jaccard index values were computed directly from the graph using Pansel on default settings, using a window size of 1 kilobasepairs. Red markers indicate position of centromeres. Values shown are rolling averages over 1,000 bins. The Jaccard index ranges from 0 (no conservation) to 1 (maximum conservation) and is computed based on pairwise comparisons of paths through the graph. This analysis shows a similar trend to the phastcons analysis in the current study, with conservation in general decreasing from the chromosome ends towards centromeres.

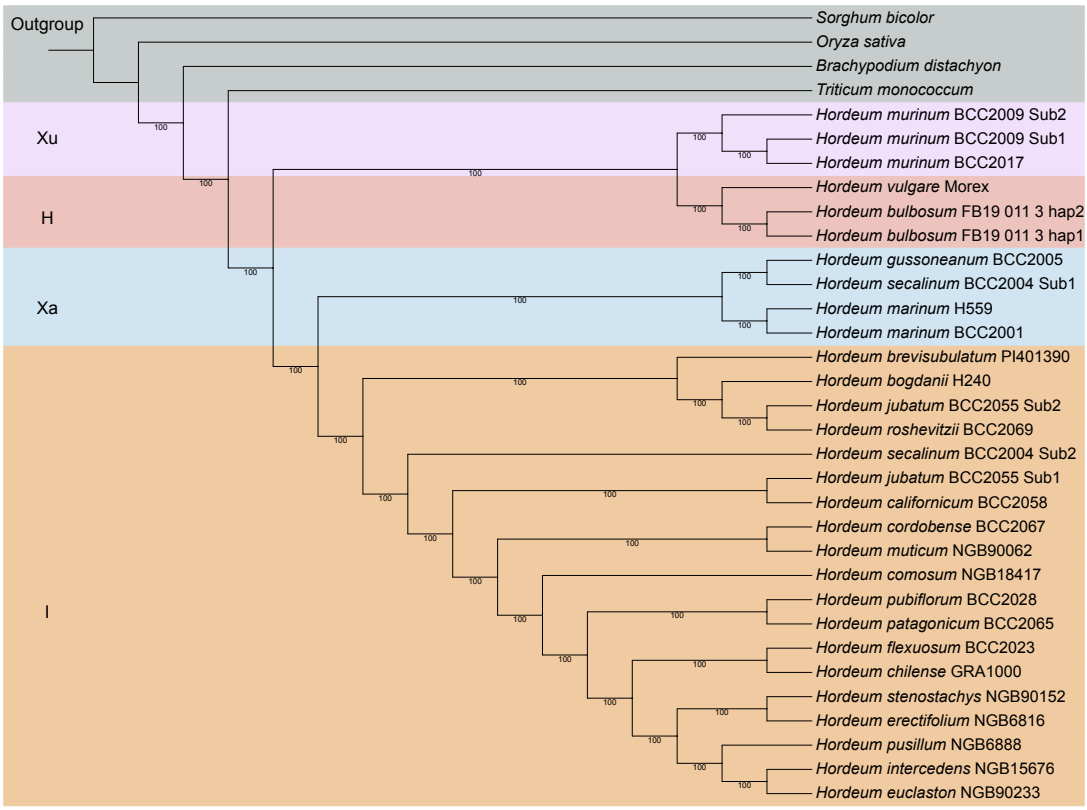

Supplementary Figure 30: Phylogenetic tree constructed by concatenated genome-wide single-copy genes. Bootstrap support values (ranging from 100 to 0) are shown at each internal node.

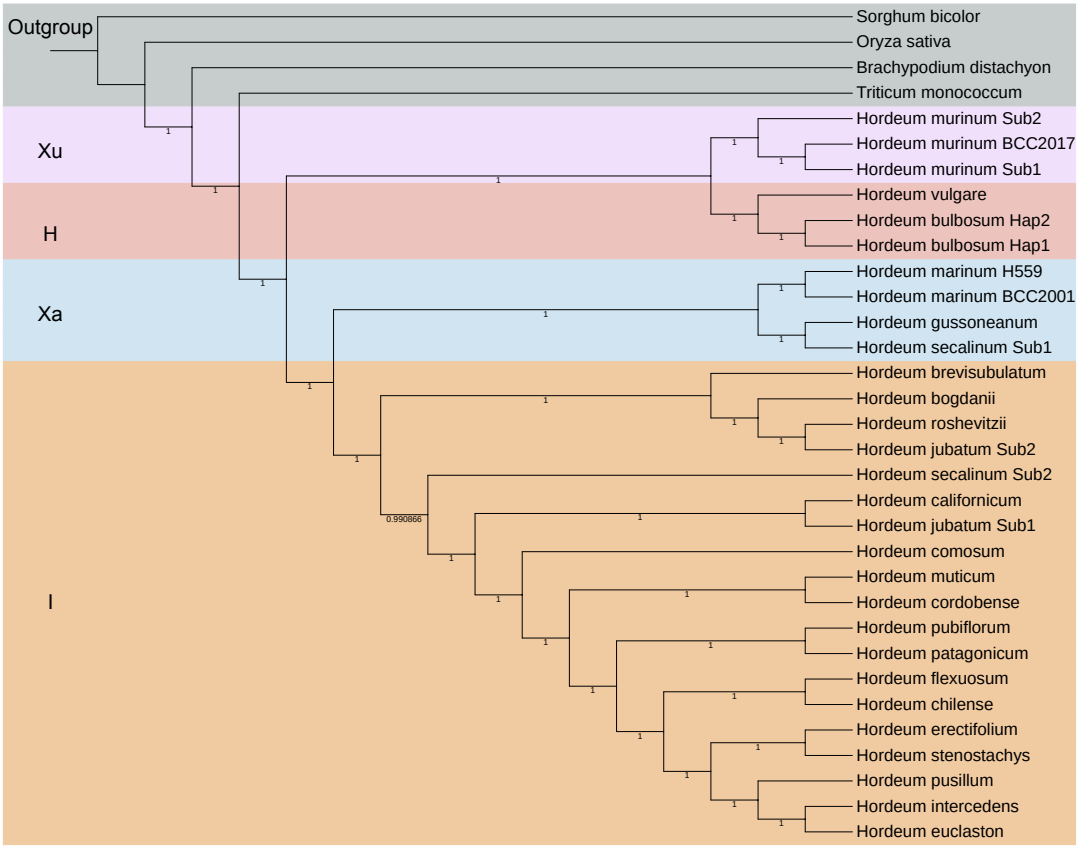

Supplementary Figure 31: Coalescence based species tree constructed by single-copy genes. Bootstrap support values (ranging from 1 to 0) are shown at each internal node.

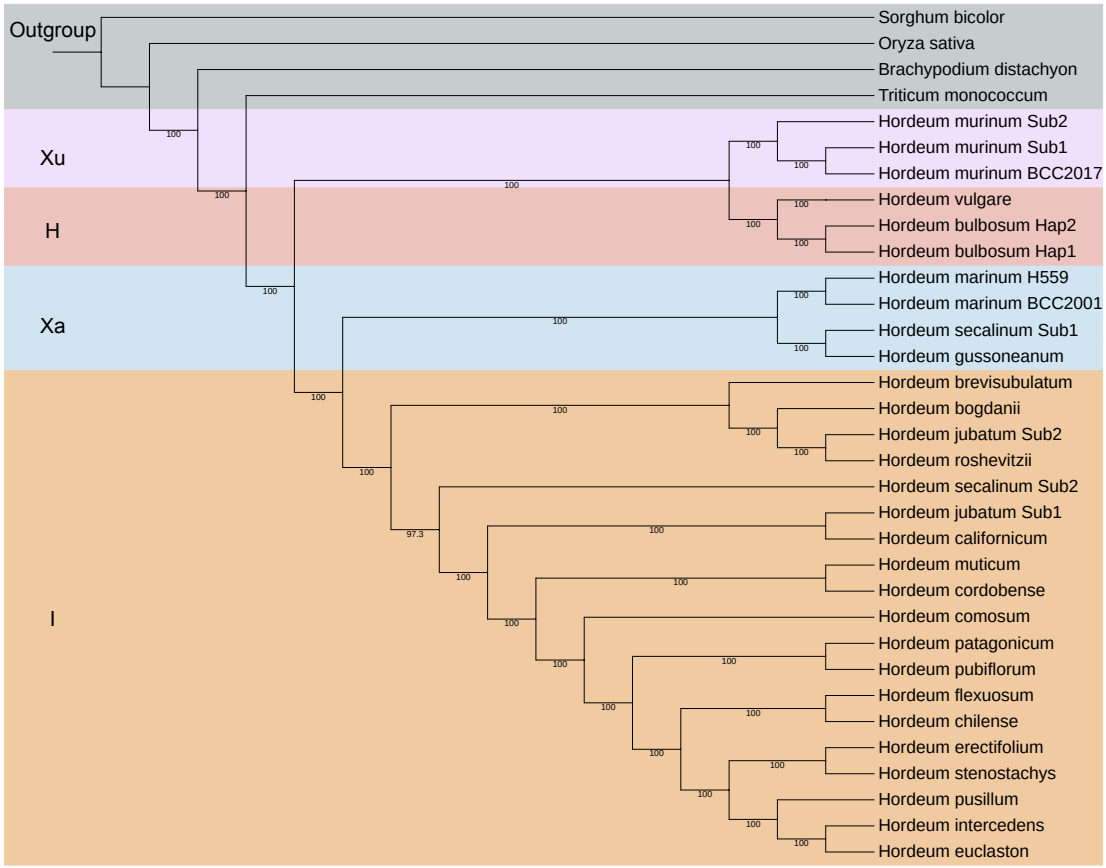

Supplementary Figure 32. Phylogenetic tree constructed using CASTER-pair based on whole-genome alignments generated by Progressive Cactus. Bootstrap support values (ranging from 100 to 0) are shown at each internal node.

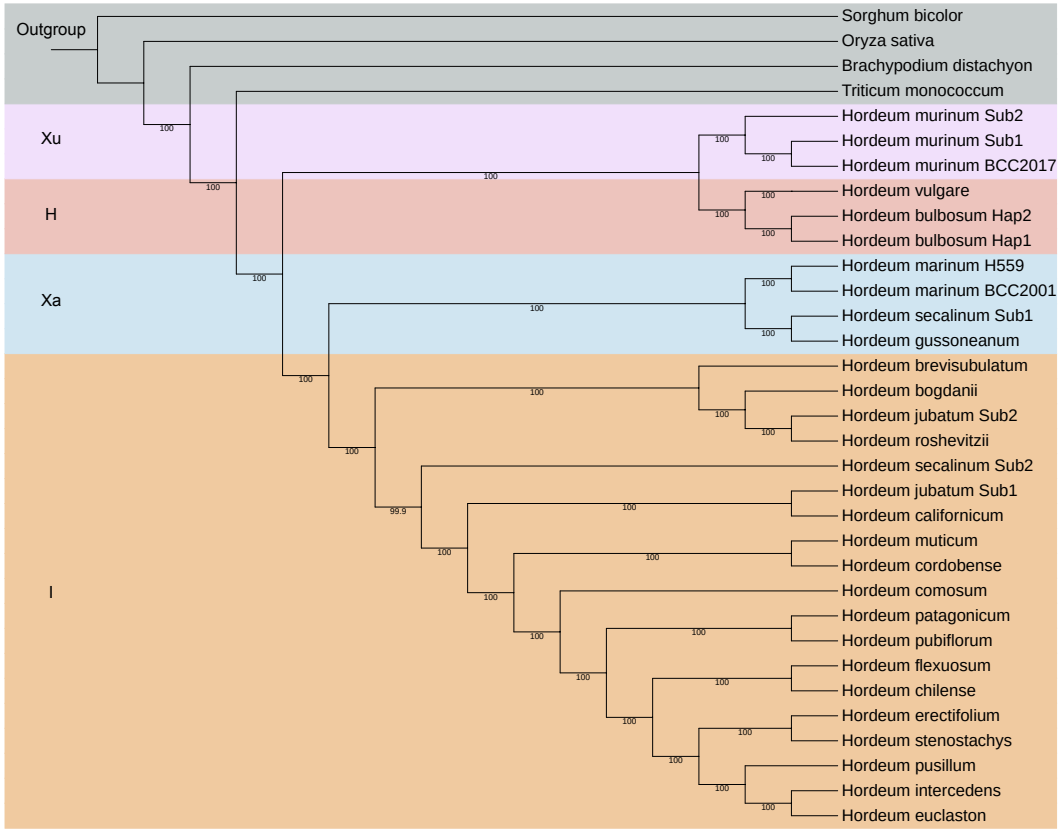

Supplementary Figure 33. Phylogenetic tree constructed using CASTER-site based on whole-genome alignments generated by Progressive Cactus. Bootstrap support values (ranging from 100 to 0) are shown at each internal node.

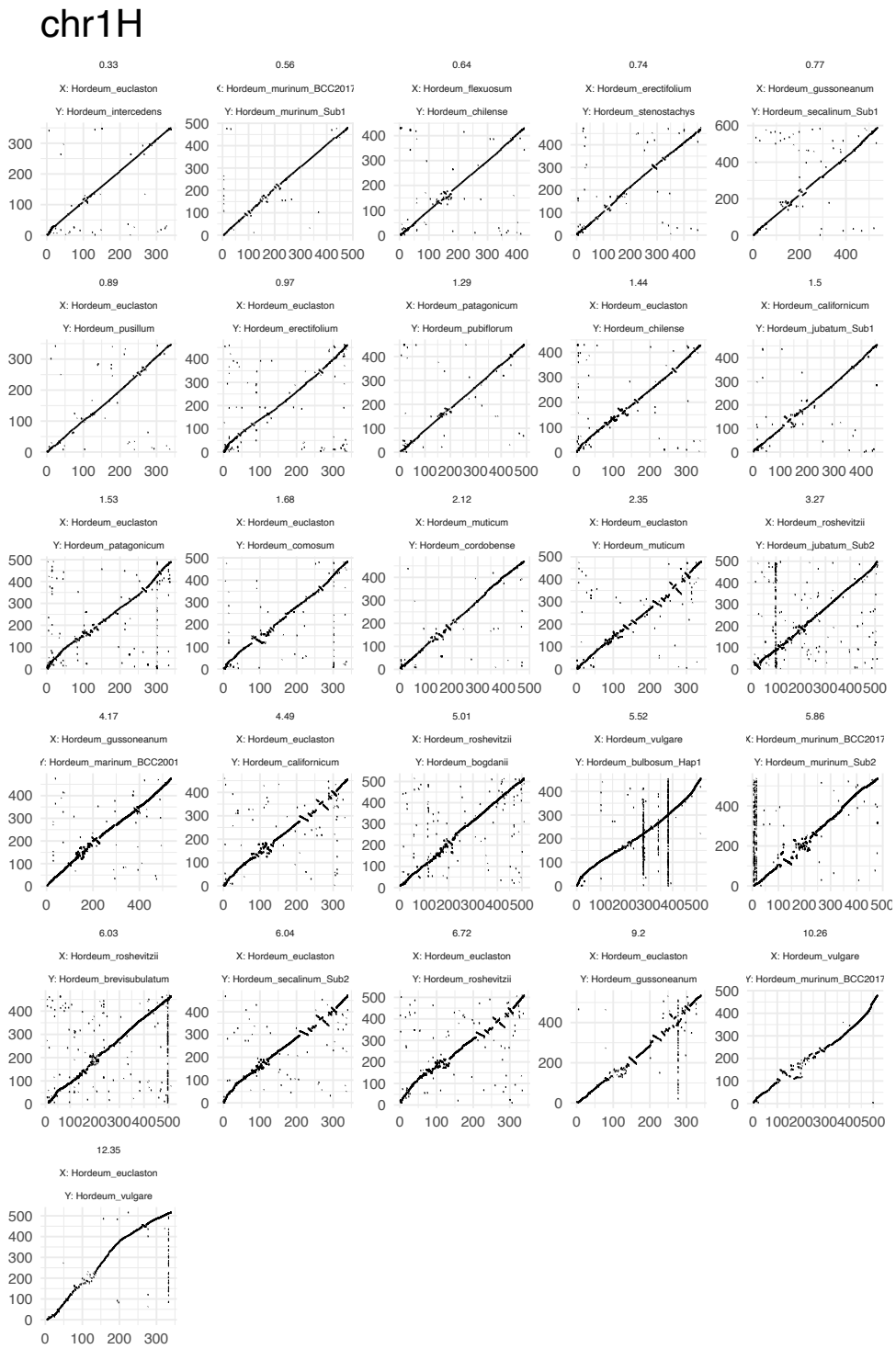

Supplementary Figure 34: Dotplot comparisons of chromosome 1H across genomes diverged at different times.

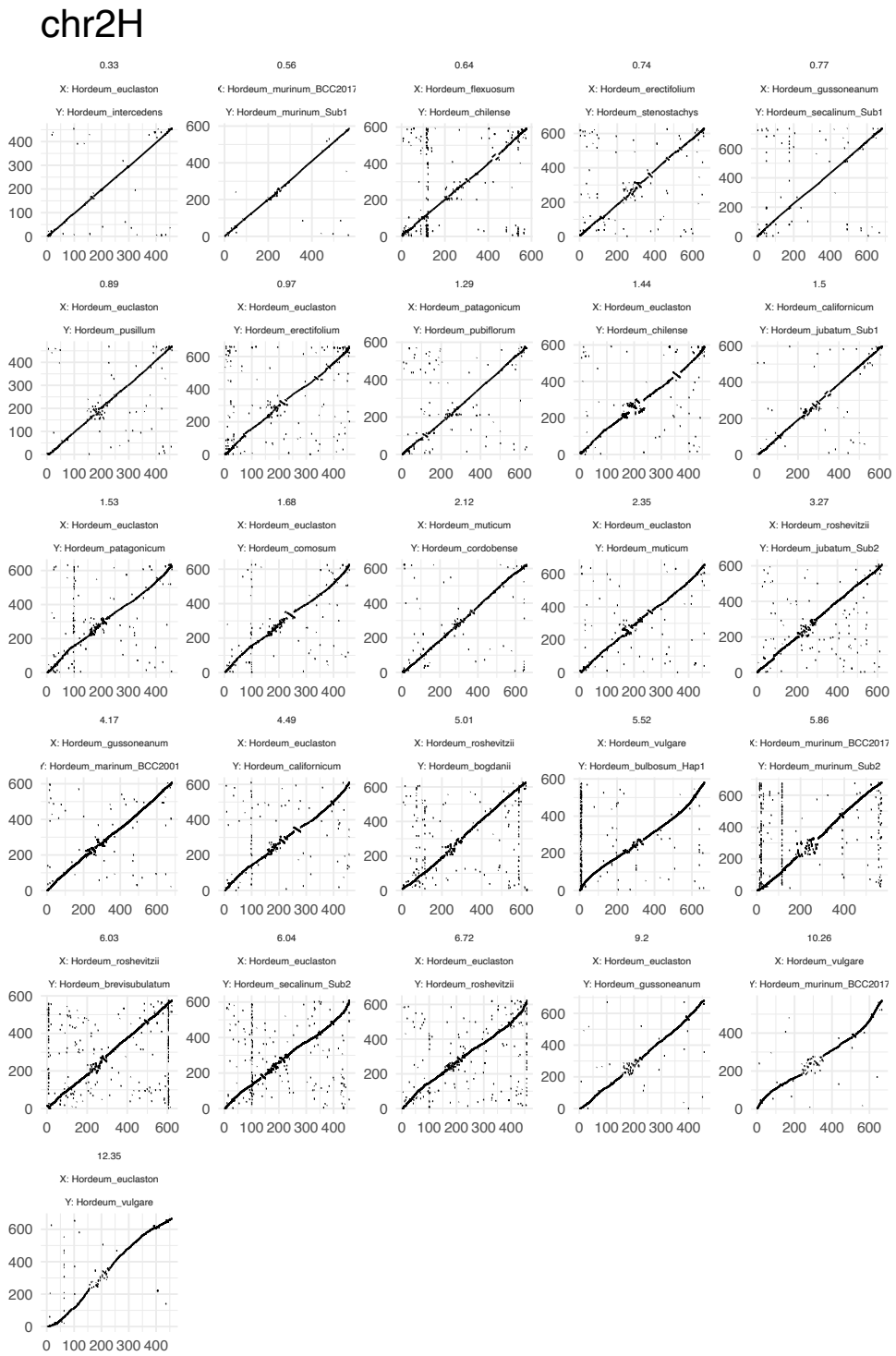

Supplementary Figure 35: Dotplot comparisons of chromosome 2H across genomes diverged at different times.

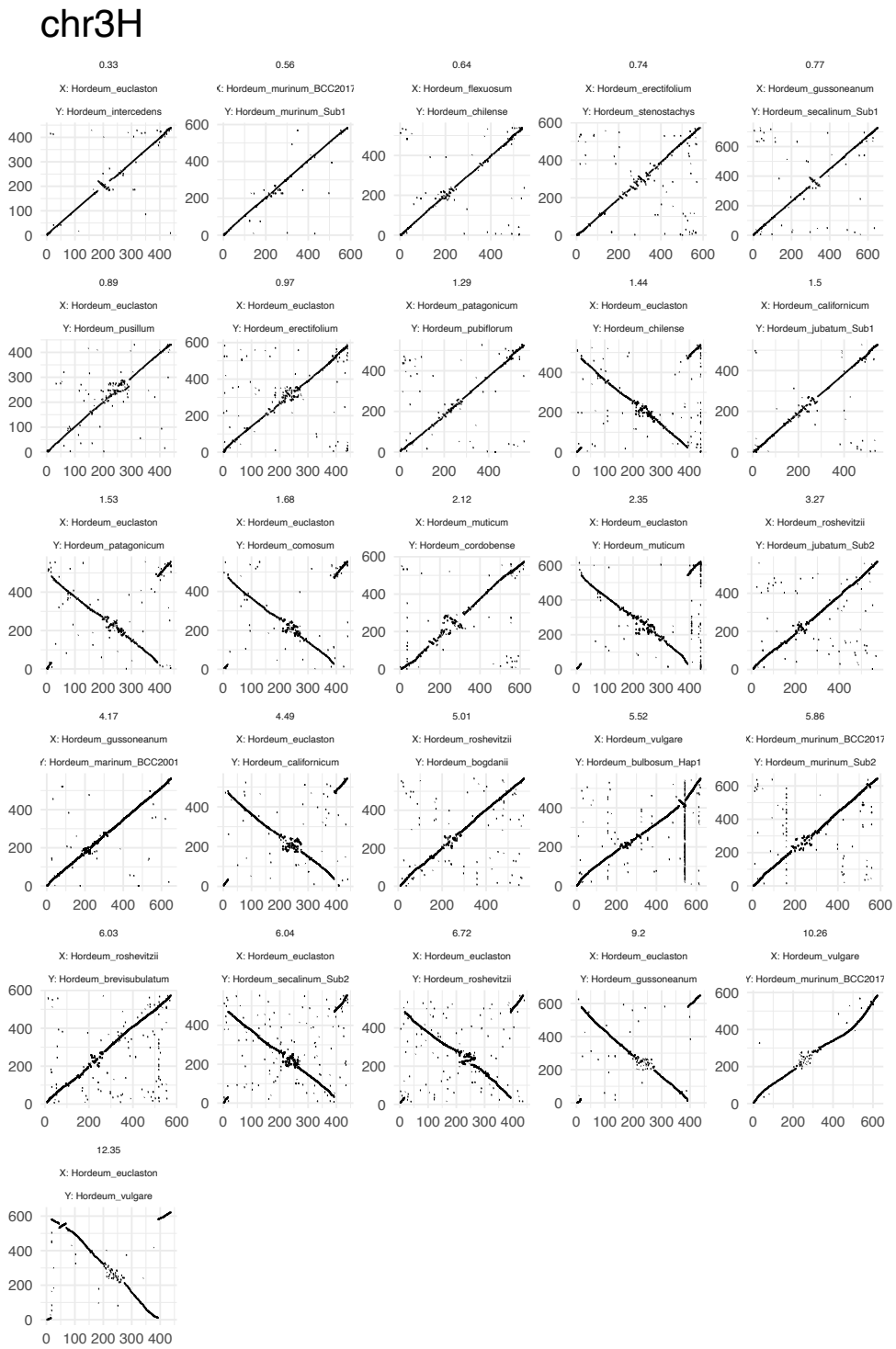

Supplementary Figure 36: Dotplot comparisons of chromosome 3H across genomes diverged at different times.

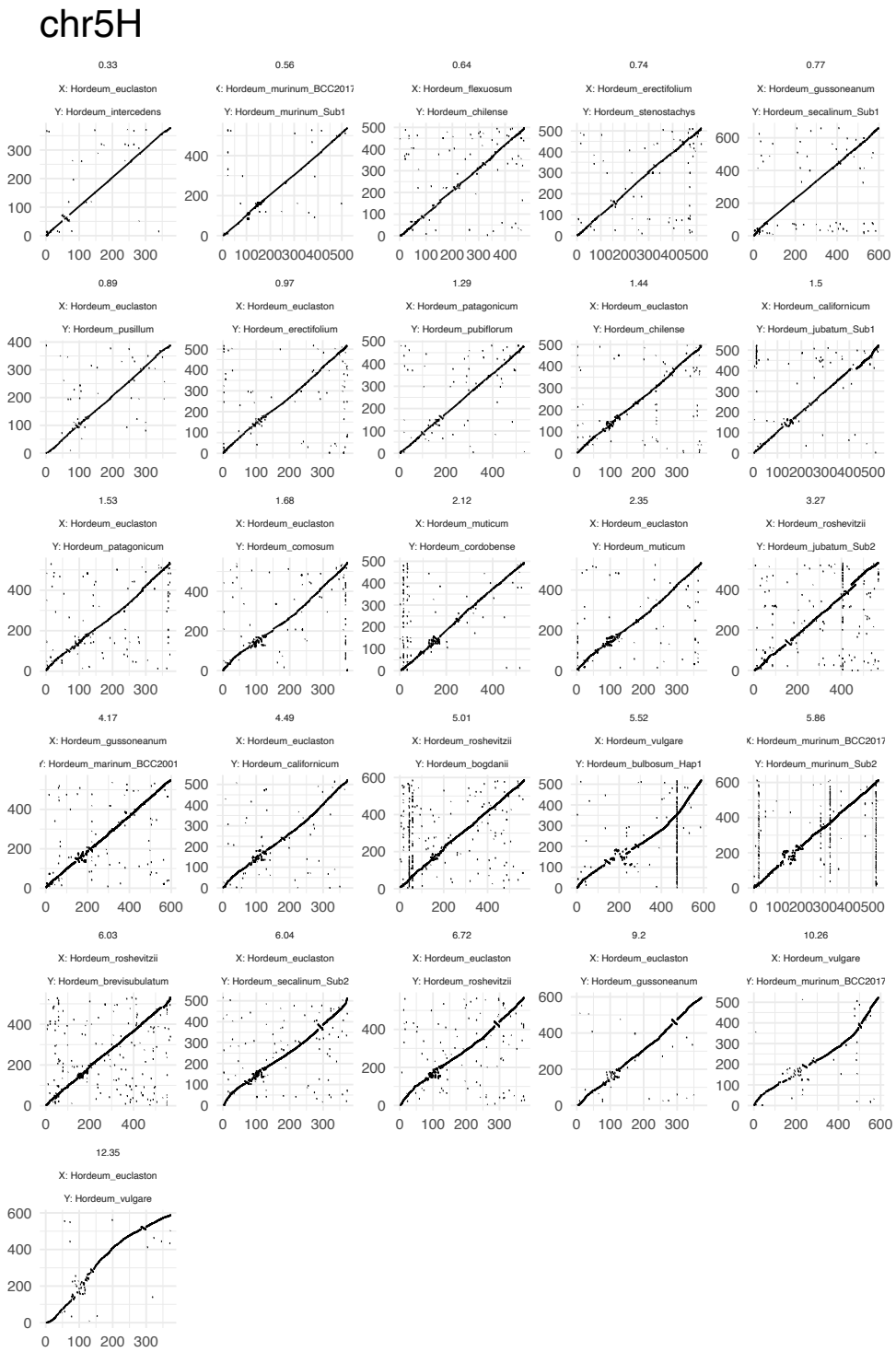

Supplementary Figure 37: Dotplot comparisons of chromosome 5H across genomes diverged at different times.

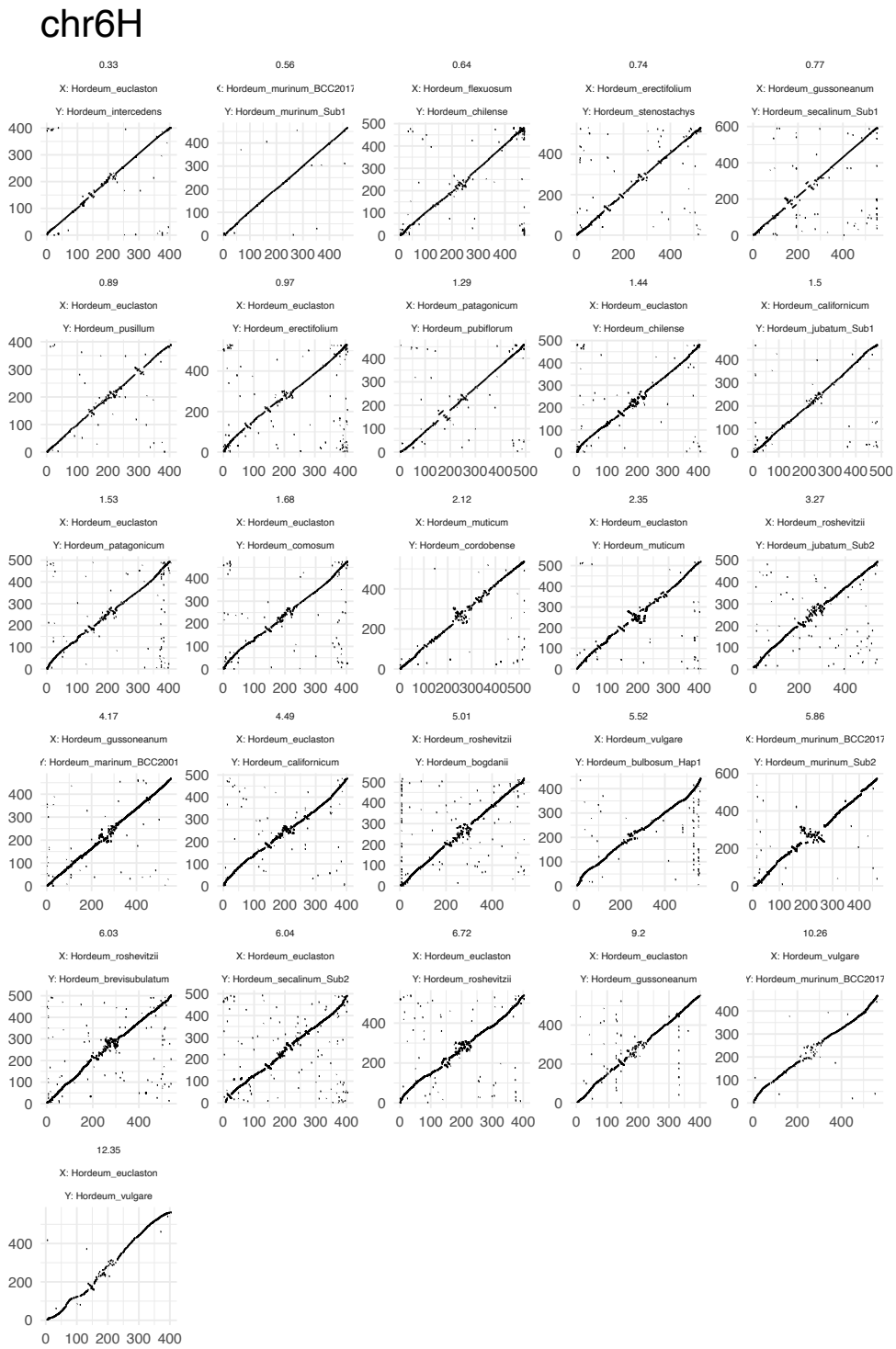

Supplementary Figure 38: Dotplot comparisons of chromosome 6H across genomes diverged at different times.

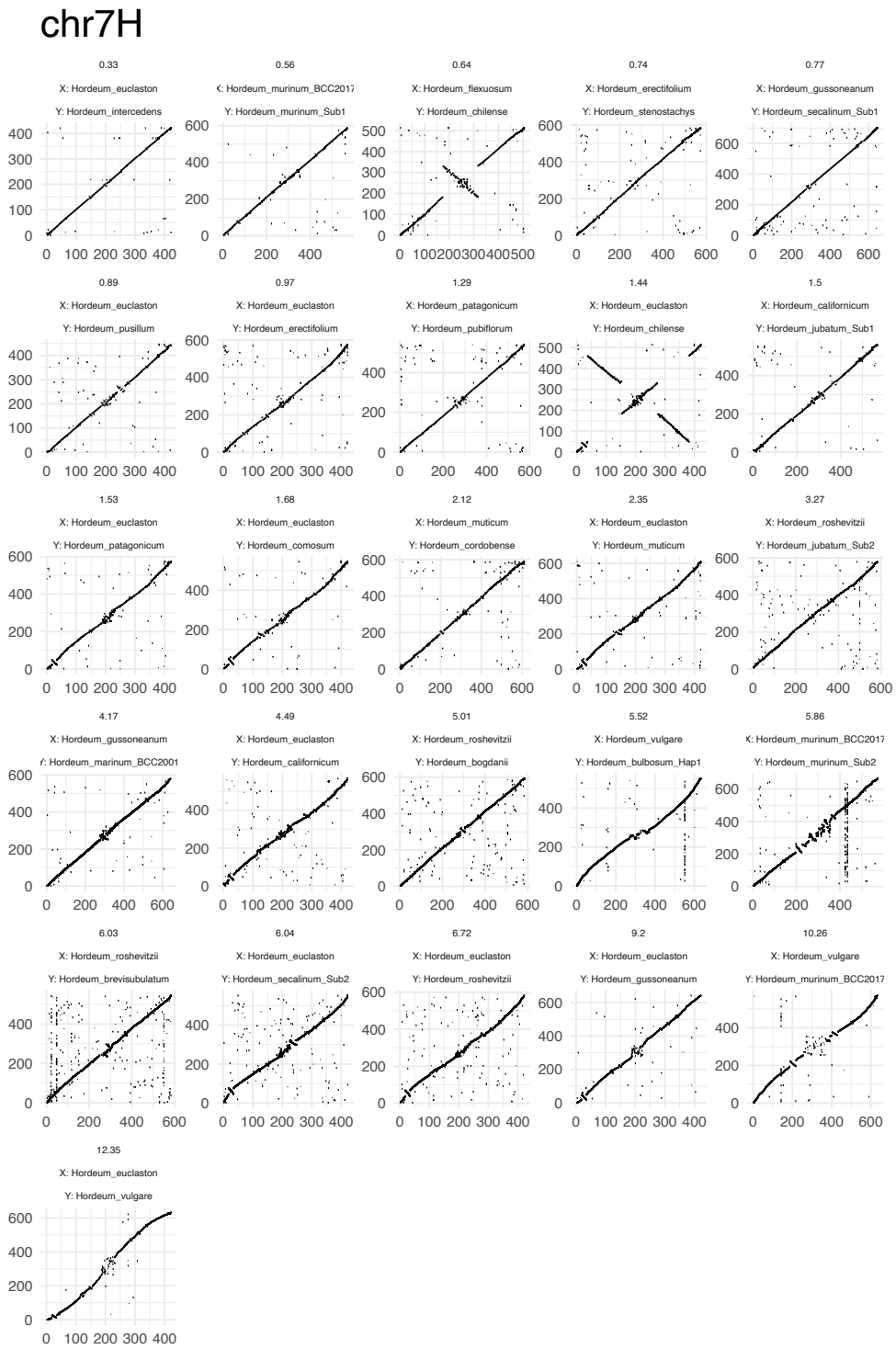

Supplementary Figure 39: Dotplot comparisons of chromosome 7H across genomes diverged at different times.

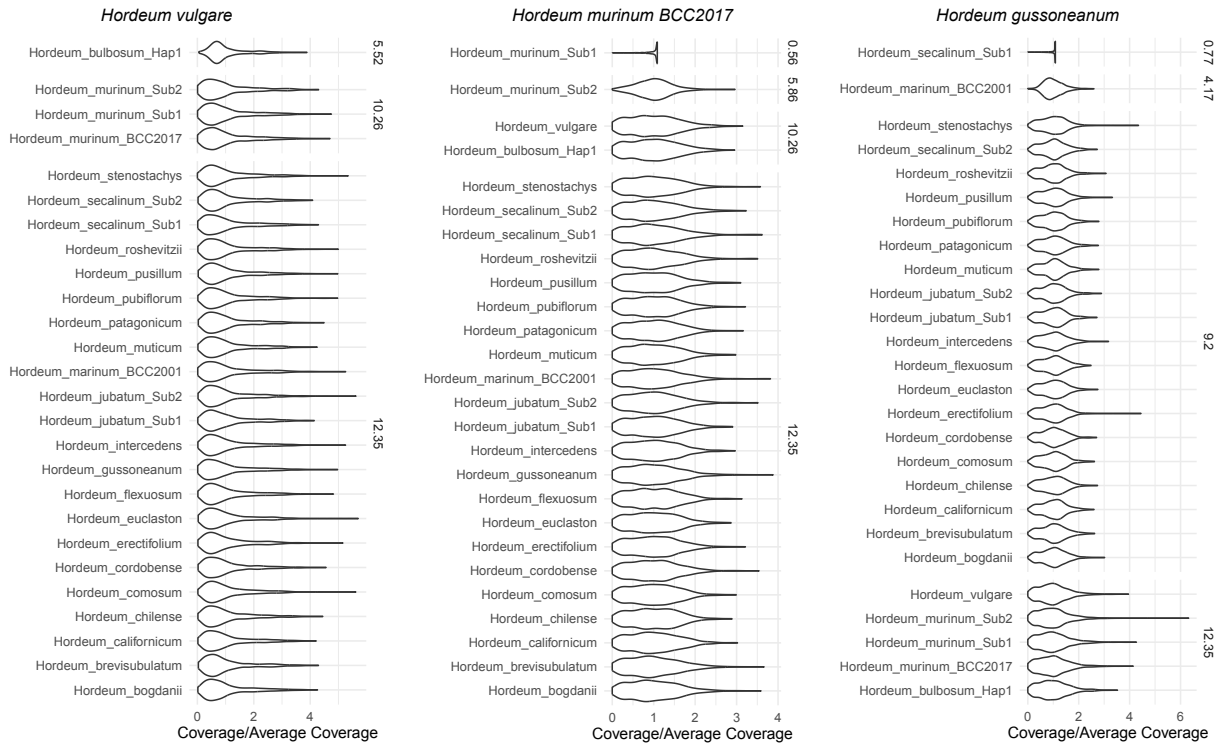

Supplementary Figure 40: Normalized coverage density plot in *H. vulgare, H. murinum* BBC2017 and *H. gussoneanum*. The right shows species ordered by divergence time in each panel.

Supplementary Figure 41: Distribution plot of genome-wide normalized coverage in *H. euclaston*. Coverage was calculated based on whole-genome alignments between *H. euclaston* and other species.

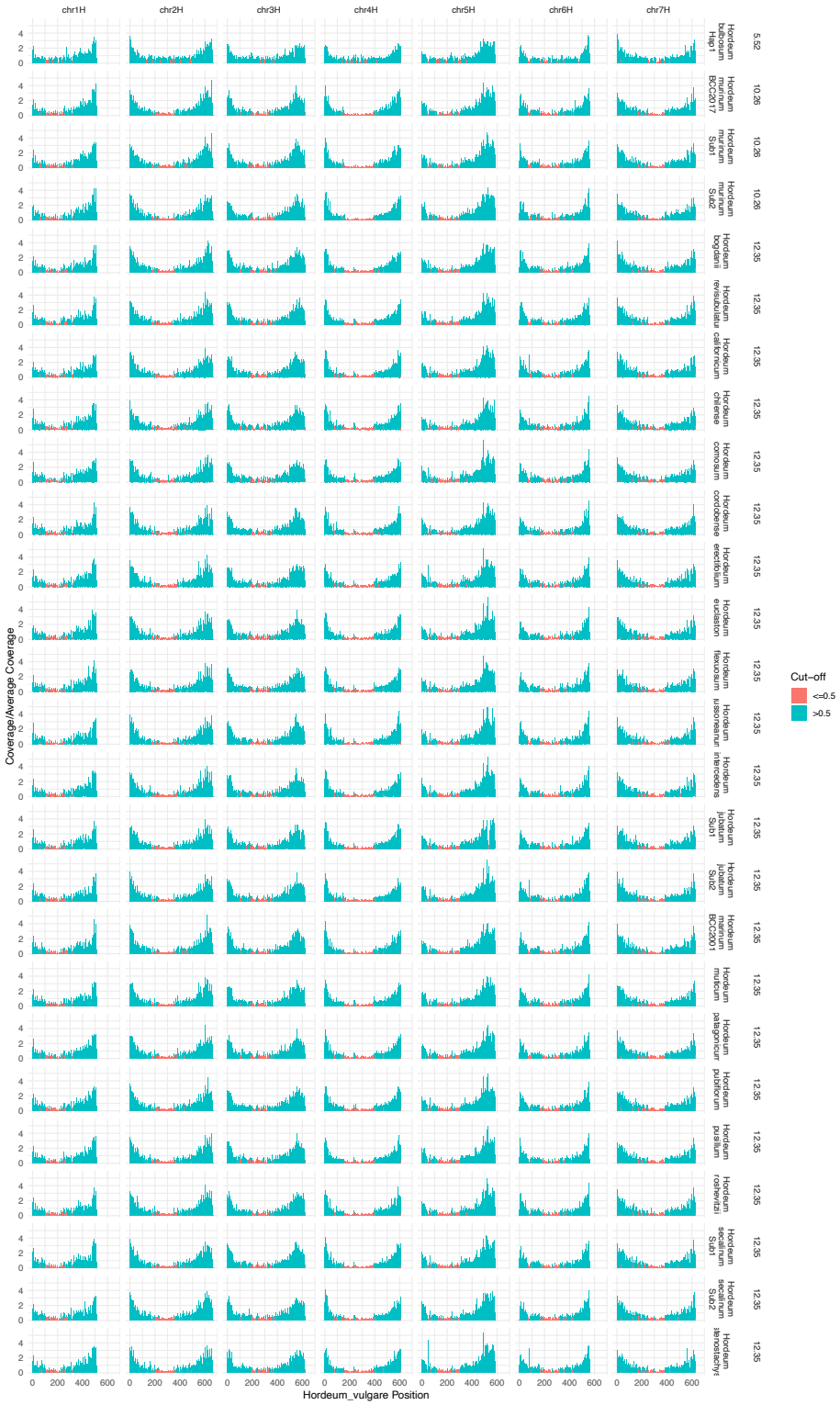

Supplementary Figure 42: Distribution plot of genome-wide normalized coverage in *H. vulgare*. Coverage was calculated based on whole-genome alignments between *H. vulgare* and other species.

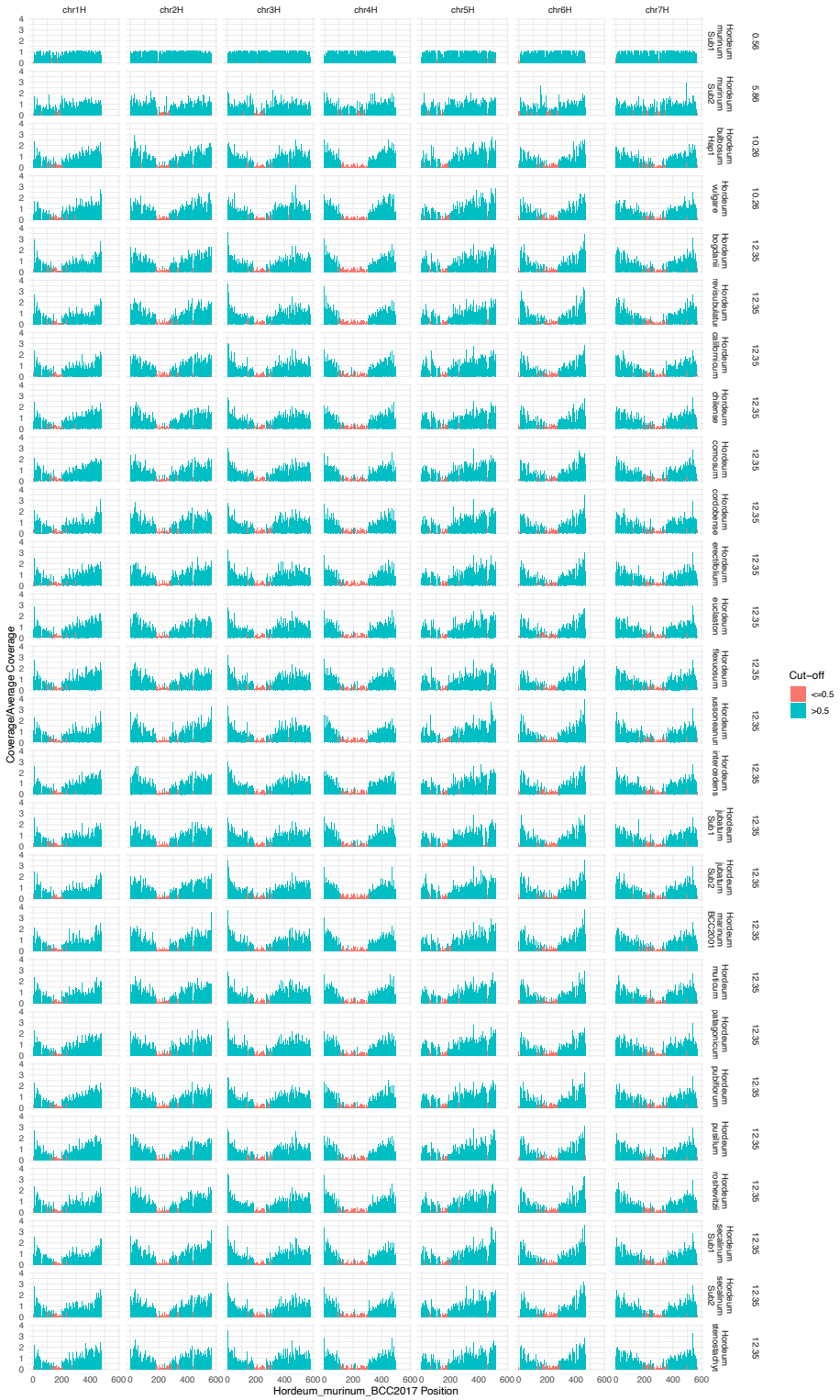

Supplementary Figure 43: Distribution plot of genome-wide normalized coverage in *H. murinum* BCC2017. Coverage was calculated based on whole-genome alignments between *H. murinum* BCC2017 and other species.

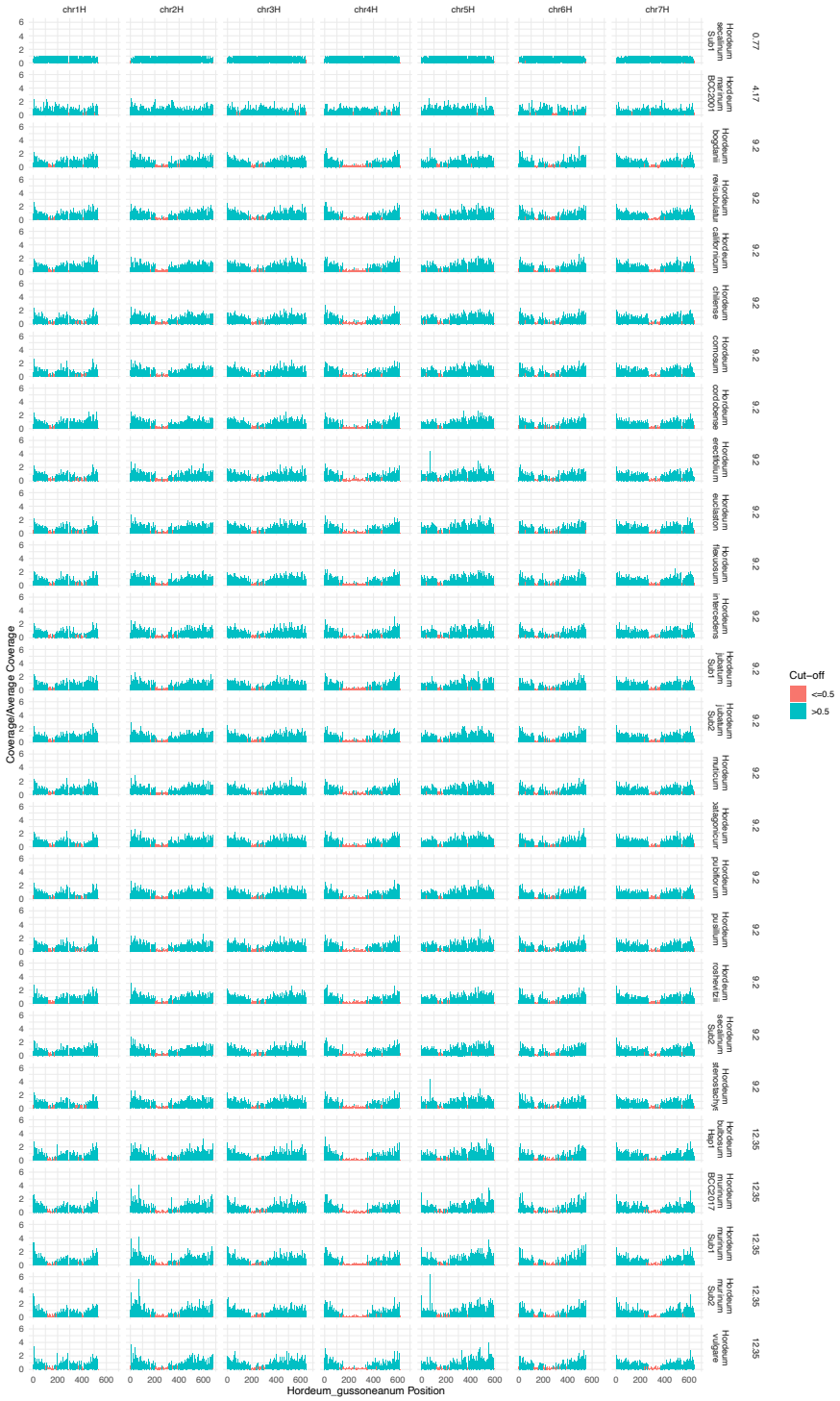

Supplementary Figure 44: Distribution plot of genome-wide normalized coverage in *H. gussoneanum*. Coverage was calculated based on whole-genome alignments between *H. gussoneanum* and other species.

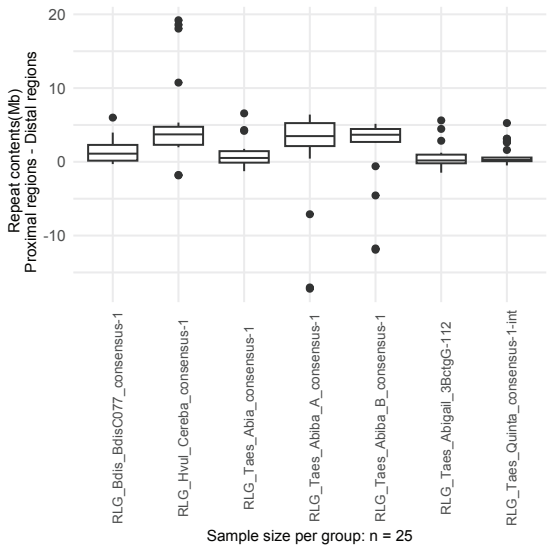

Supplementary Figure 45: Boxplot of TE family abundance differences between proximal and distal regions.

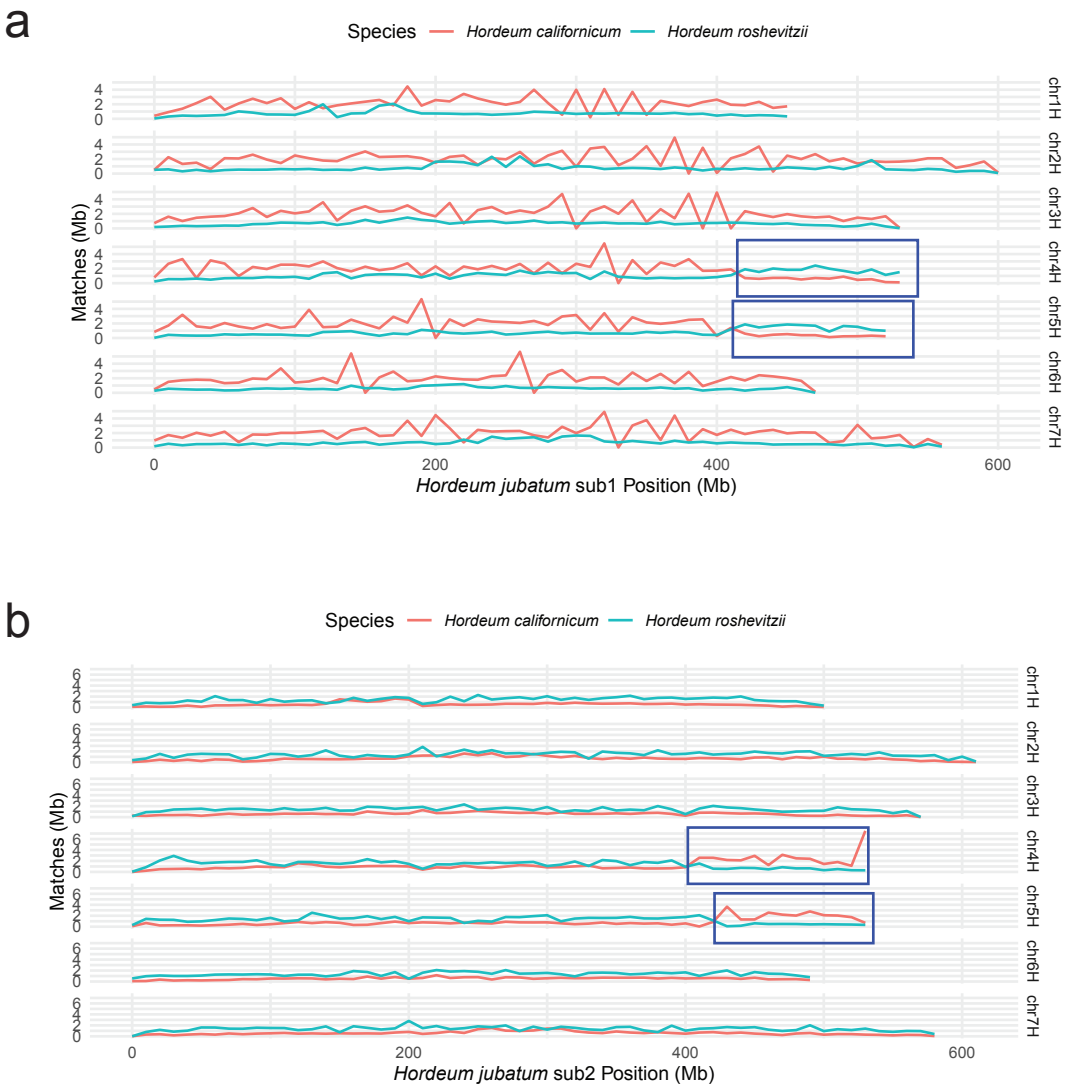

Supplementary Figure 46: Comparative distribution of matched bases between *H. jubatum* subgenomes and their diploid ancestors. (a) Distribution of matched bases per 1-Mb window between *H. jubatum* subgenome 1 and its diploid ancestors. Deep blue boxes indicate positions where tetraploid exchanges occurred. **(b)** The same analysis for *H. jubatum* subgenome 2 and its diploid ancestors.

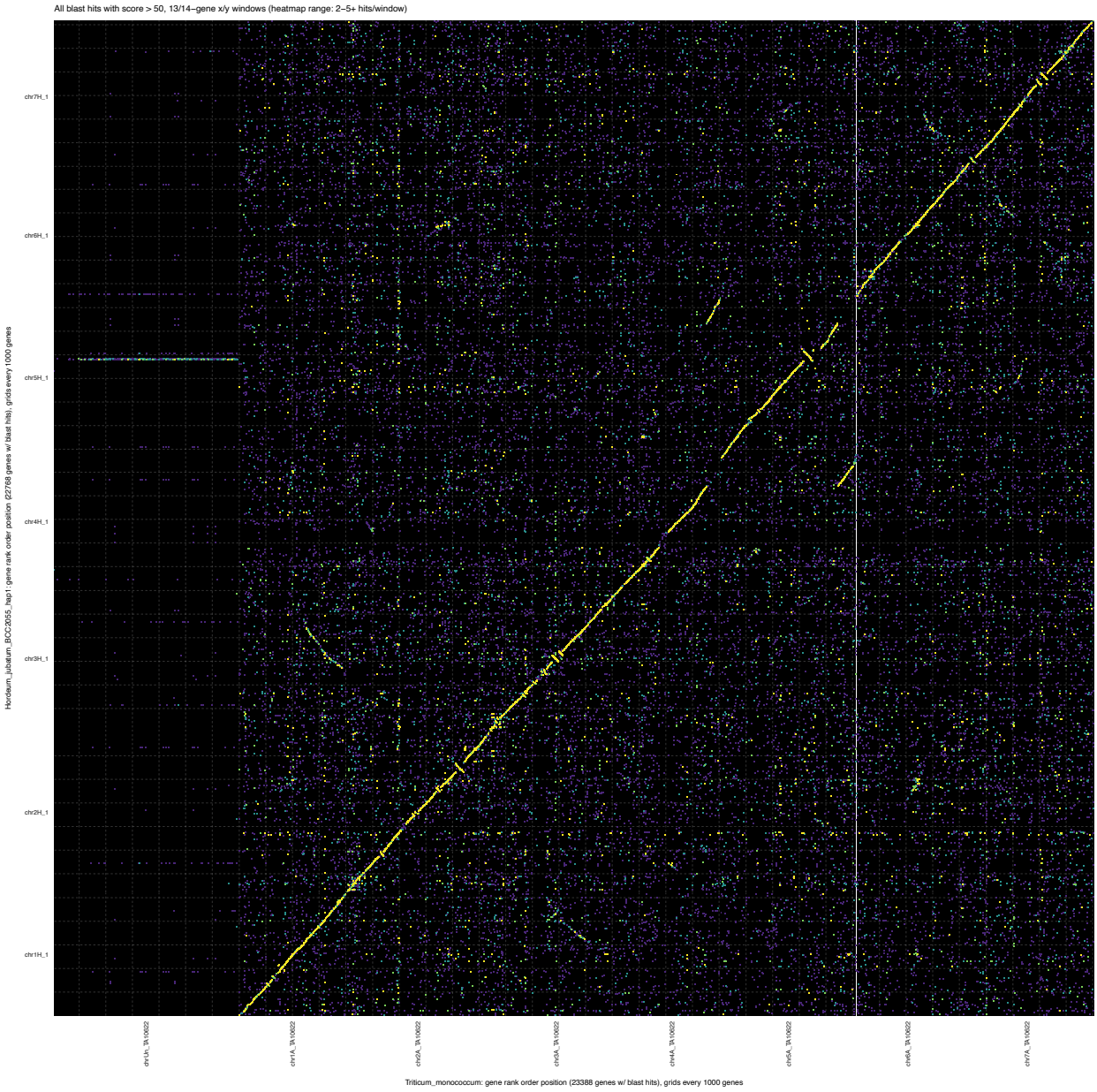

Supplementary Figure 47: Dotplot comparisons between *T. monococcum* and *H. jubatum* BCC2055 Subgenome1.

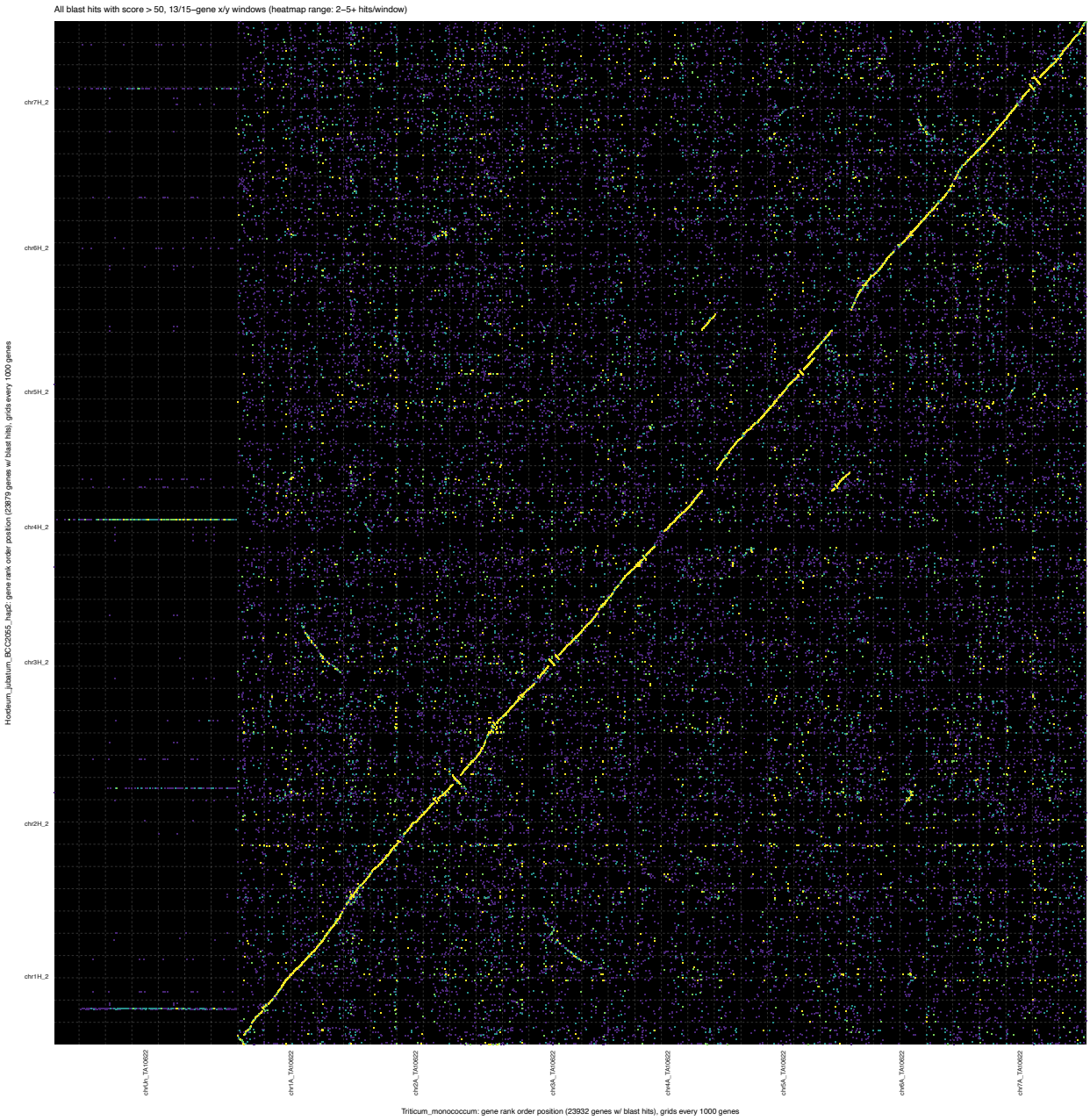

Supplementary Figure 48: Dotplot comparisons between *T. monococcum* and *H. jubatum* BCC2055 Subgenome2.